SIMULATION INVESTIGATION OF TAIL ROTOR BEHAVIOR IN DIRECTIONAL MANEUVER OF HELICOPTER

Jarosław STANISŁAWSKI
Institute of Aviation

Summary

The paper presents the simulation method for calculating the tail rotor loads and blades deflections in directional maneuver of helicopter. The simplified equation of yawing motion of helicopter was applied. The physical model consists of helicopter fuselage treated as stiffness body and tail rotor with blades modeled by elastic axes with distributed lumped masses. The rough control input of the tail rotor blade pitch allows investigate the tail rotor work including occurrence of large stall regions.

NOTATION

w, v – vertical and horizontal components of the flight speed,
θ – angle of flight path, where θ = arc tg (w/v),
φ_y – pitch angle of main rotor shaft relative to vertical line,
ε_k – built-in inclination angle of main rotor shaft relative to assembly vertical line,
α_k – fuselage angle of attack,
T_{xw}, T_{zw} – horizontal and vertical components of main rotor thrust,
G – helicopter weight,
Q_x – helicopter drag force,
N_z – fuselage lift force,
P_h – lifting force of horizontal stabilizer,
M_{yk} – aerodynamic pitching moment of fuselage,
M_{tr} – tail rotor reaction moment,
x_{sc}, z_{sc} – location of the helicopter mass center relative to the center of main rotor hub respectively in perpendicular and parallel direction to the axis of the main rotor shaft,
h_n – distance between the center of main rotor hub and point of helicopter hanging as a equivalent pendulum,
h_{a1}, x_{ha1} – location of application point of fuselage aerodynamic forces relative to the center of main rotor hub,
l_h, l_v, l_{tr} – respectively distances of the horizontal stabilizer, fin and tail rotor shaft to the axis of the main rotor shaft.

1. INTRODUCTION

A simulation program for computing the tail rotor loads in varying conditions of helicopter flight was developed. The airflow terms of the tail rotor blades could be rapidly changed in helicopter maneuvers or due to side wind gusts. The necessity of more precisely prediction of the tail rotor characteristics in dynamic maneuvers was expressed in CAA (*Civil Aviation Authority*) analysis concerning the investigations of helicopter accidents. The events due to loss of directional control were collected in special groups [1], [2]. In some cases, the mechanical structure failures or blade collision with external matter or ground were excluded as the reasons for decline of the tail rotor thrust. The loss of directional control of helicopter may occur as the result of aerodynamic disturbances of tail rotor blades airflow. According to the CAA evaluation the time margin for pilot to recognize the situation of growing danger is no longer than 2 seconds. The lack of proper pilot reaction may lead to direction instability of helicopter.

The tail rotor simulation program was developed as a connection of procedure for calculating the equilibrium of helicopter in steady flight state and code used to obtain loads of main rotor blades in given flight conditions [3], [4]. For the tail rotor condition the horizontal axis of whirling is assumed. The helicopter fuselage is treated as rigid body while the tail rotor blades are modeled as the elastic axis with attached lumped masses. The new version of program code allows for simulation investigations of the tail rotor work in the hover or level flight conditions including changes of blade pitch angles and side wind gust velocity. The input data file for calculations was prepared according characteristic of light helicopter IS-2. The simulation procedure has been partly verified by comparing the computed results with wind tunnel measurements of the scaled IS-2 main rotor model.

2. HELICOPTER EQUILIBRIUM CONDITIONS

Taking into consideration the equilibrium conditions of helicopter for given flight regime the required thrust of tail rotor and its blade pitch angle must be define. For the equilibrium at steady level flight the calculations of cyclic and collective pitch of main rotor blades, fuselage pitch and roll angles are also necessary.

According to flight speed the required power as well the forces and moments acting on helicopter are calculated. In program code the load equilibrium conditions are treated as fulfilled if at the next step of iteration the difference for the fuselage pitch angle values and roll angle values are less than 0.1 degree. For the known components of main rotor thrust and moments and known value of the tail rotor thrust it is possible to define, necessary to create them, swashplate deflections relative to the axis of main rotor shaft and to define the blade pitch angle of tail rotor. As the input data for calculations were used the characteristics of IS-2 light helicopter with start mass of 785 kg.

In accordance with equilibrium condition of helicopter loads in longitudinal plane the following method of computing the swashplate deflection can be derived. The scheme of forces and moments acting on helicopter in longitudinal plane is shown in Fig. 1.

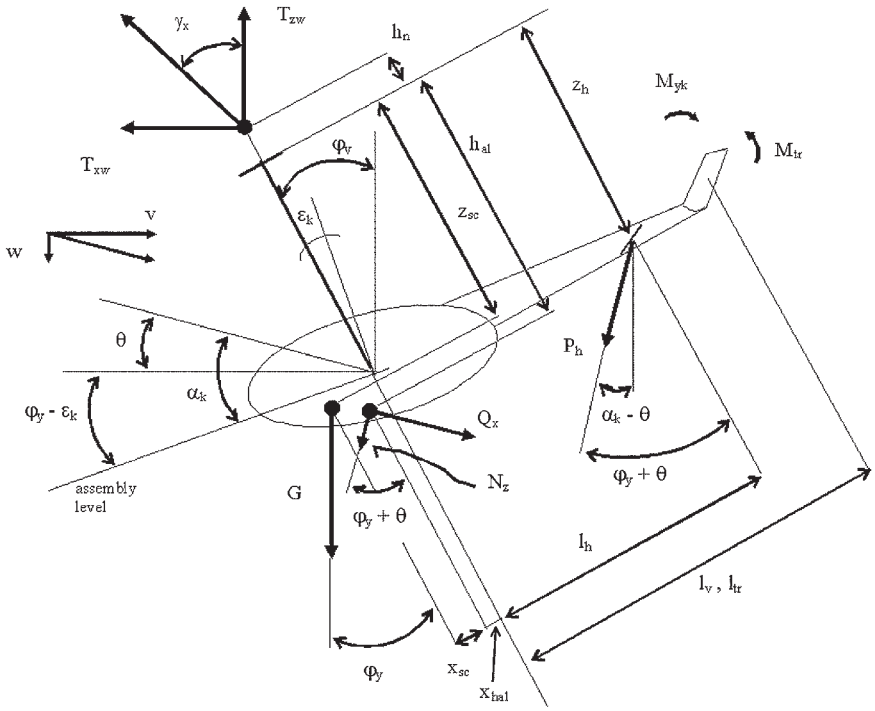

Fig. 1. Scheme of helicopter loads in longitudinal plane

For flight at the fuselage angle of attack α_k the lifting force N_z and drag Q_x of fuselage equals:

$$Q_x = \frac{1}{2}\rho \cdot \left(v^2 + w^2\right) \cdot \Pi R_w^2 \cdot c_{xk}\left(\alpha_k\right), \tag{1}$$

$$N_z = \frac{1}{2}\rho \cdot \left(v^2 + w^2\right) \cdot \Pi R_w^2 \cdot c_{zk}\left(\alpha_k\right), \tag{2}$$

where

ρ – air density,

$c_{xk}\left(\alpha_k\right), c_{zk}\left(\alpha_k\right)$ – coefficients of fuselage drag and lift,

R_w – main rotor radius.

According to the equilibrium of forces conditions the components of the main rotor thrust can be define:

$$T_{xw} = Q_x \cos(\alpha_k - \theta) - N_z \sin(\alpha_k - \theta) - P_h \sin(\alpha_k - \theta), \tag{3}$$

$$T_{zw} = Q_x \sin(\alpha_k - \theta) + N_z \cos(\alpha_k - \theta) + P_h \cos(\alpha_k - \theta) + G. \tag{4}$$

The fuselage pitch angle (pitch angle of main rotor shaft axis) is calculated due to the fuselage moments equation which is determined relative to imaginary point of helicopter hanging as the physical pendulum. The fuselage moment equation is following:

$$\begin{aligned} &G(h_n + z_{sc})\sin\phi_y - Gx_{sc}\cos\phi_y - P_h l_h \cos(\phi_y + \theta) + P_h(h_n + z_h)\sin(\phi_y + \theta) \\ &+ N_z(h_n + h_{a1})\sin(\phi_y + \theta) - N_z x_{ha1}\cos(\phi_y + \theta) - Q_x(h_n + h_{a1})\cos(\phi_y + \theta) \\ &- Q_x x_{ha1}\sin(\phi_y + \theta) + M_{yk} + M_{tr} = 0. \end{aligned} \tag{5}$$

Deflections of the helicopter control system are derived as below. The collective pitch angle of the main rotor blades can be computed in accordance with following equation:

$$\vartheta_o = \frac{c_T^* + \vartheta_s\left(t_4 + 0{,}5\mu_o^2 t_2\right) + \lambda_o\left(t_2 + 2\mu_o^2\right)}{t_3 + 0{,}5\mu_o^2 t_1}, \tag{6}$$

where meaning of component symbols is following:

c_T^* – coefficient of the main rotor thrust,

ϑ_s – geometrical twist of main rotor blade,

μ_o, λ_o – dimensionless coefficients of airflow through rotor disk,

t_1, t_2, t_3, t_4 – constants concerning taper shape of main rotor blade and determined by following expression:

$$t_n = 4\int_{\bar{r}_1}^{\bar{r}_2} \frac{b}{b_o}\bar{r}^{(n-1)} d\bar{r}, \tag{7}$$

where

$\bar{r}_1, \bar{r}_2$ – relative radiuses, aerodynamic non-active at root and tip of blade,

b_o – theoretical blade chord at rotor hub,

b – current blade chord.

Other components of equation (6) depend on state of flight and rotor parameters. The thrust coefficient equals:

$$c_T^* = \frac{8\,T}{\rho\,\Omega^2 R_w^3\, a\, k_w b_{07}}, \tag{8}$$

where

Ω – rotational speed of main rotor,

R_w – radius of main rotor,

$a = dc_z/d\alpha$ – derivative of lift coefficient to attack angle for rotor blade airfoil,

k_w – number of main rotor blades,

b_{07} – blade chord at radius r = 0.7 R_W.

The rotor advance ratio (in plane of rotation) and the rotor inflow ratio (positive downward through plane of rotation) depend on the advance and inflow ratio through plane of rotor blade tips μ_{Tw} and λ_{Tw} a_1 and depend on the blade coning angle a_1.

Rotor advance ratio in plane of rotation equals:

$$\mu_o = -\lambda_{Tw} \sin a_1 + \mu_{Tw} \cos a_1 \tag{9}$$

and rotor inflow ratio normal to plane of rotation:

$$\lambda_o = \lambda_{Tw} \cos a_1 + \mu_{Tw} \sin a_1, \tag{10}$$

where

$$\lambda_{Tw} = \frac{v \sin(\gamma_x + \theta) + v_i}{\Omega R_w}, \tag{11}$$

$$\mu_{Tw} = \frac{v \cos(\gamma_x + \theta)}{\Omega R_w}, \tag{12}$$

$\gamma_x + \theta$ – angle of free flow on rotor,

v_i – induced velocity in rotor plane.

The induced velocity in the plane of the rotor for the condition of forward flight condition is equal:

$$v_i = \sqrt{\sqrt{\frac{v^4}{4} + \left(\frac{T}{2\pi R_w^2 \rho \chi} \right)^2} - \frac{v^2}{2}}, \tag{13}$$

where

χ – coefficient of blade tip loss.

Appearing in equations (9) and (10) angle a_1 of blade coning can be calculated in compliance with following expression:

$$a_1 = \frac{\mu_o (2 t_3 \vartheta_o - 2 t_4 \vartheta_s - \lambda_o t_2)}{t_4 - 0,25 \mu_o^2 t_2}. \tag{14}$$

The constant component a_0 of blade coning is define as below:

$$a_o = \frac{(t_4 + 0,5 \mu_o^2 t_2) \vartheta_o - (t_5 + 0,5 \mu_o^2 t_3) \vartheta_s - t_3 \lambda_o}{\gamma^*}, \tag{15}$$

where blade mass constant equals

$$\gamma^* = \frac{8 I_{fl.hin.}}{\rho R_w^4 a b}, \tag{16}$$

$I_{fl.hin.}$ – blade moment of inertia about the flapping hinge.

Using the equations (15) and (13) one can calculate the b_1 angle – lateral tilt of blade coning:

$$b_1 = \frac{\mu_o t_3 a_o + t_4 K \bar{v}}{t_4 + 0,25 \mu_o^2 t_2}, \tag{17}$$

where $\bar{v}$ – non-dimensional induced velocity

$$\bar{v} = \frac{v_i}{\Omega R_w}, \tag{18}$$

and coefficient K of induced velocity distribution at rotor disk:

$$K = \frac{4\mu_{Tw}}{3\left(1,2\lambda_{Tw} + \mu_{Tw}\right)}. \tag{19}$$

After computing the blade flapping angles a_1 and b_1 relatively to the plane of constant blade pitch it is possible to define the angles of blade flapping a_{1y} and b_{1y} in relation to swashplate plane:

$$a_{1y} = \frac{a_1 + \bar{k}_w b_1}{1 + \bar{k}_w^2}, \tag{20}$$

$$b_{1y} = \frac{b_1 - \bar{k}_w a_1}{1 + \bar{k}_w^2}, \tag{21}$$

where – flap and pitch coefficient of rotor blade.

Using the results obtained for lateral equilibrium condition: the tail rotor thrust T_{tr} and fuselage roll angle φ_x in next step are calculated the angles of swashplate deflection θ_{tx} and θ_{ty} in relation to the axis of the main rotor shaft:

– pitch angle of swashplate

$$\theta_{ty} = \frac{\left(a_{1y} - \phi_y + \gamma_x\right)D_1 - \left(\phi_x - {T_{tr}}/{T} - b_{1y}\right)}{D_1^2 + D_2^2}, \tag{22}$$

– roll angle of swashplate

$$\theta_{tx} = \frac{b_{1y} - \phi_x + {T_{tr}}/{T} - D_2\theta_{ty}}{D_1}, \tag{23}$$

where D_1, D_2 coefficients of geometrical transmission in blade pitch control links:

$$D_1 = \frac{\bar{D}_1 + \bar{k}_w \bar{D}_2}{1 + \bar{k}_w^2}, \tag{24}$$

$$D_2 = \frac{\bar{D}_2 - \bar{k}_w \bar{D}_1}{1 + \bar{k}_w^2}. \tag{25}$$

The amount of power required by rotor P_w can be define as the sum of the fan power component P_{fan} to force the air flow through the rotor disk and the drag power component P_{drag} to rotate blades:

$$P_w = P_{fan} + P_{drag}. \tag{26}$$

The fan power component equals:

$$P_{fan} = T \cdot V_{Aw}, \tag{27}$$

where

T – the main rotor thrust,

V_{Aw} – airflow velocity through rotor (normal to rotor disk).

Due to expression (11) V_{Aw} is given

$$V_{Aw} = v\sin\left(\gamma_x + \theta\right) + v_i. \tag{28}$$

The blade drag component of power consists of two parts:

$P_{drag.\_1}$ – power required for rotating the rotor,

$P_{drag.\_2}$ – power required to move the whole rotor at velocity v.

$$P_{drag} = P_{drag\_1} + P_{drag\_2}, \tag{29}$$

where

$$P_{drag\_1} = \frac{1}{8}\rho\left(\Omega \cdot R_w\right)^3 R_w \cdot k_w \cdot b_{07} \cdot c_{xw} \cdot \left(t_4 + 0{,}5 \cdot \mu_{Tw}^2 \cdot t_2\right), \tag{30}$$

$$P_{drag\_2} = \frac{1}{8}\rho\left(\Omega \cdot R_w\right)^2 R_w \cdot k_w \cdot b_{07} \cdot v \cdot \left(0{,}425\mu_{Tw}^2 \cdot t_1 \cdot c_{xow} + \mu_{Tw} \cdot t_2 \cdot c_{xw} + 3\mu_{Tw}^3 \cdot c_{xw}\right), \tag{31}$$

and the mean value of blade airfoil drag coefficient for rotor disk area is dependent on rotor thrust coefficient:

$$c_{xw} = c_{xow} \cdot \left(1 + \frac{\left(a \cdot c_T^*\right)^2}{t_3^2 + \mu_{Tw}^2\left(2 \cdot t_2^2 + t_1 \cdot t_3\right)}\right). \tag{32}$$

The tail rotor thrust required to balance the moments acting to helicopter fuselage can be calculated according to following formula:

$$T_{tr} = T_{tr1} + \frac{M_{zk}}{l_{tr}} + P_{yk} \cdot \frac{x_{ha1}}{l_{tr}} - P_{yv} \cdot \frac{l_v}{l_{tr}}, \tag{33}$$

where

T_{tr1} –the tail rotor thrust balancing the main rotor reaction moment

$$T_{tr1} = \frac{P_w}{\Omega \cdot l_{tr}}, \tag{34}$$

M_{zk} – aerodynamic yawing moment of fuselage (without fin)

$$M_{zk} = \frac{1}{2}\rho\, v^2 \cdot \Pi\, R_w^3 \cdot c_{mzk}\left(\beta_k\right), \tag{35}$$

P_{yk} – aerodynamic lateral force of fuselage (without fin)

$$P_{yk} = \frac{1}{2}\rho\, v^2 \cdot \Pi\, R_w^2 \cdot c_{yk}\left(\beta_k\right), \tag{36}$$

P_{yv} – lifting force of fin (lateral)

$$P_{yv} = \frac{1}{2}\rho\, v^2 \cdot S_v \cdot a_v \cdot \left(\beta_k + \beta_v\right), \tag{37}$$

S_v – area of fin,

a_v – derivative of fin lift coefficient to cyv fin angle of attack,

β_k – fuselage sideslipe angle,

β_v – assembly angle of fin.

The angle of helicopter roll relative to vertical can be calculated after defining the distances d_1, d_2, d_3, d_4 (Fig. 2) between the points of application of forces acting in lateral plane the equivalent point of hanging the helicopter treated as the physical pendulum. The height h_n of equivalent hanging point above the main rotor hub according the following formula is equal:

$$h_n = \frac{k_w \cdot S_{pp} \cdot \left(\Omega R_w\right)^2 \cdot l_o}{2 \cdot T \cdot R_w^2}, \tag{38}$$

where

l_o – flapping hinge offset to axis of main rotor shaft,

S_{pp} – mass static moment of main rotor blade relative to flapping hinge.

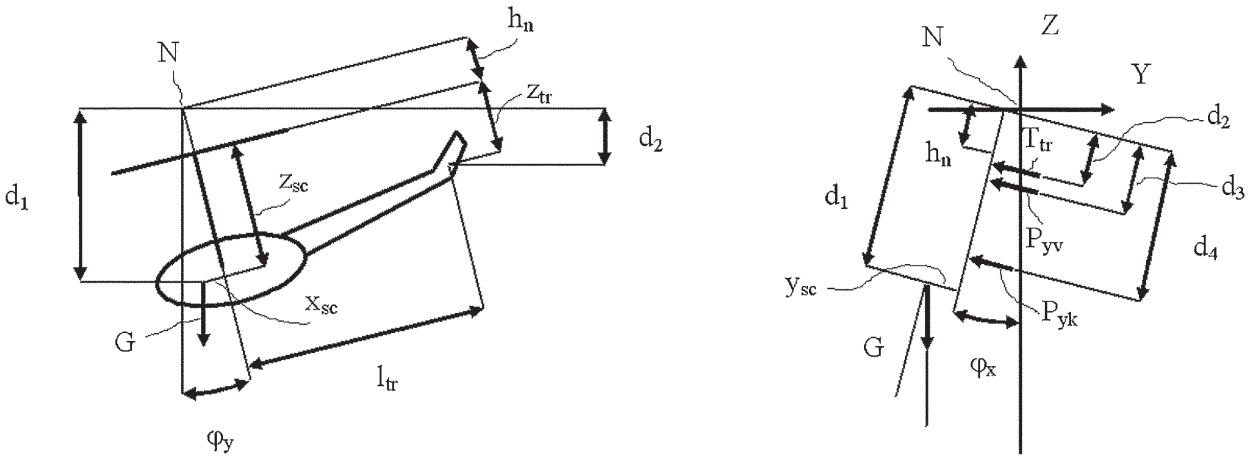

Fig. 2. Scheme of equilibrium of forces and moments in lateral plane, N – equivalent point position of hanging the helicopter

The distances of application points for forces acting in lateral plane due to the equivalent hanging point of helicopter are equal(Fig. 1 and Fig. 2):

$$d_1 = \left(h_n + z_{sc}\right) \cdot \cos\phi_y + x_{sc} \cdot \sin\phi_y, \tag{39a}$$

$$d_2 = \left(h_n + z_{tr}\right) \cdot \cos\phi_y - l_{tr} \cdot \sin\phi_y, \tag{39b}$$

$$d_3 = \left(h_n + z_v\right) \cdot \cos\phi_y - l_v \cdot \sin\phi_y, \tag{39c}$$

$$d_4 = \left(h_n + h_{a1}\right) \cdot \cos\phi_y + x_{ha1} \cdot \sin\phi_y. \tag{39d}$$

Taking into consideration the distances d_1, d_2, d_3, d_4 the roll angle φ_x of helicopter can be calculated:

$$\phi_x = \frac{T_{tr} \cdot d_2 + P_{yv} \cdot d_3 + P_{yk} \cdot d_4 - G \cdot y_{sc}}{G \cdot d_1}, \tag{40}$$

where

y_{sc} – lateral location of helicopter center of mass.

For defining the pitch angle of the tail rotor blades ϑ_{tr} allowing in given flight conditions to obtain required value of the tail rotor thrust T_{tr} the same procedure can be used as applied for calculation of collective pitch of the main rotor blades. In analogy to (6)÷(15) formulas the following parameters can be calculated.

The tail rotor thrust coefficient c^*_{Ttr}:

$$c^*_{Ttr} = \frac{8\,T_{tr}}{\rho\;\Omega^2_{tr} R^3_{tr}\, a_{tr}\, k_{tr} b_{07\_tr}}, \tag{41}$$

where

Ω_{tr} – rotational speed of the tail rotor shaft,

R_{tr} – tail rotor radius,

$a_{tr} = dc_{ztr}/d\alpha$ – derivative of lift coefficient to attack angle for the tail rotor blade airfoil,

k_{tr} – number of blades of the tail rotor,

b_{07_tr} – chord of the tail rotor blade at radius $r = 0.7\ R_{tr}$.

The induced velocity of the tail rotor for the forward flight conditions at speed v is equal:

$$v_{itr} = \sqrt{\sqrt{\frac{v^4}{4} + \left(\frac{T_{tr}}{2\pi\, R^2_{tr}\rho\;\chi_{tr}}\right)^2} - \frac{v^2}{2}}, \tag{42}$$

where

χ_{tr} – coefficient of tip losses for the tail rotor.

The non-dimensional coefficients of tail rotor the advance ratio and the inflow ratio (in plane and through plane of rotation) are dependent on the tail rotor blade coning angle a_{1tr} and the advance and inflow ratio relative to the tail rotor blade tips μ_{Ttr} and λ_{Ttr}.

The tail rotor advance ratio in its plane of rotation equals:

$$\mu_{otr} = -\lambda_{Ttr}\sin a_{1tr} + \mu_{Ttr}\cos a_{1tr}, \tag{43}$$

and the tail rotor inflow ratio normal to plane of rotation equals

$$\lambda_{otr} = \lambda_{Ttr}\cos a_{1tr} + \mu_{Ttr}\sin a_{1tr}, \tag{44}$$

where

$$\lambda_{Ttr} = \frac{v\cdot\sin\left(\beta_k - a_{1tr}\right) + v_{itr}}{\Omega_{tr}\cdot R_{tr}}, \tag{45}$$

$$\mu_{Ttr} = \frac{v\cdot\cos\left(\beta_k - a_{1tr}\right)}{\Omega_{tr}\cdot R_{tr}}, \tag{46}$$

$(\beta_k - a_{1tr})$– angle of free flow on the tail rotor disk,

v_{itr} – induced velocity in the tail rotor plane.

The pitch angle of the tail rotor blades can be defined according to the following formula:

$$\lambda_{Ttr} = \frac{v\cdot\sin\left(\beta_k - a_{1tr}\right) + v_{itr}}{\Omega_{tr}\cdot R_{tr}}, \tag{47}$$

where

– geometrical twist of the tail rotor blade,

– geometrical parameters dependent to the taper shape of the tail rotor blade given by following formula:

$$\mu_{Ttr} = \frac{v\cdot\cos\left(\beta_k - a_{1tr}\right)}{\Omega_{tr}\cdot R_{tr}}, \tag{48}$$

where

$\overline{r}_{1tr}$, $\overline{r}_{2tr}$ – relative radiuses, aerodynamic non-active at root and tip of the tail rotor blade,

b_{otr} – theoretical blade chord at the centre of tail rotor hub,

b_{tr} – current chord of the tail rotor blade.

Existing in formulas (43)÷(48) coefficient a_{1tr} – the conning angle of the tail rotor blades can be define as follows:

$$a_{1tr} = \frac{\mu_{otr}\left(2t_{3tr}\cdot\vartheta_{tr} - 2t_{4tr}\cdot\vartheta_{str} - \lambda_{otr}\cdot t_{2tr}\right)}{t_{4tr} - 0,25\mu_{otr}^{2}\cdot t_{2tr}}. \tag{49}$$

The pitch angle of the tail rotor blade ϑ_{tr} is defined at iteration process as the accuracy condition for calculating the coning angle a_{1tr} of the tail rotor blades will be fulfilled:

$$\left|\left(a_{1tr}\right)_{n+1} - \left(a_{1tr}\right)_{n}\right| \le \varepsilon\ . \tag{50}$$

3. THE TAIL ROTOR MODEL

For the investigation of the tail rotor problems the simulation program code prepared to compute loads of helicopter main rotor may find application. The tail rotor can be treated as the main rotor but with axis of its shaft tilt to horizontal position. The physical model of the tail rotor, shown in Fig. 3, consists of blades and hub arms. The program code involves the single blade analysis, where at given time step, the parameters of motion and loads only for one blade rotor are calculated. The loads of the rotor shaft are defined after collecting the results for azimuth positions relating to other rotor blades.

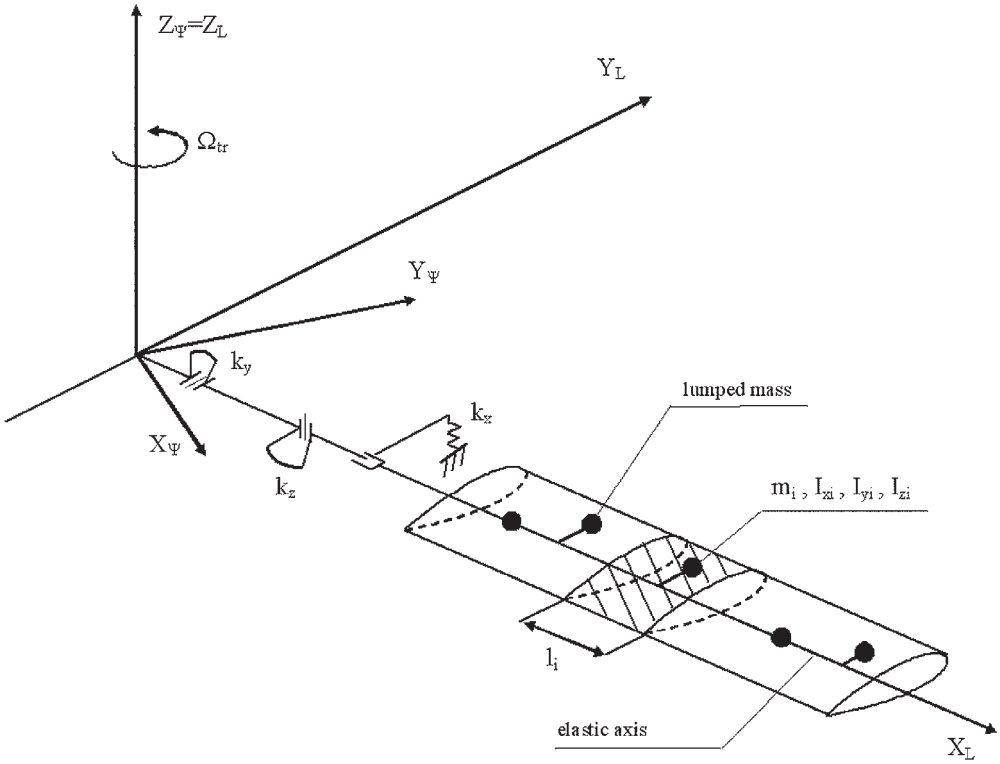

Fig. 3. The physical model of rotor blade; segment in length l_i, mass m_i and inertial moments I_{xi}, I_{yi}, I_{zi} was replaced by lumped mass

The physical model of blade has been defined taking the following assumptions:

- the mass distribution of the real blade is replaced by lumped mass system,
- the elastic axis represents the stiffness characteristics of the blade,
- segments of the elastic axis connect the blade cross sections with attached lumped masses,
- blade elastic axis can be mutually twisted and bent in-plane and out of rotor plane direction,
- blade is connected with hub by set of elastic elements or hinges in-plane, out of plane and axial,
- shaft of main rotor is treated as ideal stiffness,
- in non-deformed state the elastic axis is in the same localization as the pitch axis of blade.

4. EQUATION OF MOTION FOR DEFORMED BLADE

The mathematical model of rotor is formed by the equations of motion of blades treated as the elastic axes. The equations of motion can be derived using Lagrange formula:

$$\frac{d}{dt}\left(\frac{\partial T}{\partial \dot{q}_i}\right)-\frac{\partial T}{\partial q_i}+\frac{\partial U}{\partial q_i}=Q_i \qquad \text{i = 1, ... , n} \tag{51}$$

The potential energy of elastic axis being twisted and bent in two planes equals:

$$U=\int_0^L \frac{M_Y^2}{2EJ_Y}dx+\int_0^L \frac{M_Z^2}{2EJ_Z}dx+\int_0^L \frac{M_S^2}{2GJ_X}dx. \tag{52}$$

The bending and twisting moments acting at cross sections of elastic axis can be defined due to its deformations out of plane *y*, in plane z and twist angle φ :

$$M_Y=EJ_Y\frac{d^2z}{dx^2},\ M_Z=EJ_Z\frac{d^2y}{dx^2},\ M_S=GJ_X\frac{d\varphi}{dx}. \tag{53}$$

After substitution formulas (53) into equation (52) the expression for potential energy is given in the following form:

$$U=\frac{1}{2}\int_0^L EJ_Y\left(\frac{d^2z}{dx^2}\right)^2dx+\frac{1}{2}\int_0^L EJ_Z\left(\frac{d^2y}{dx^2}\right)^2dx+\frac{1}{2}\int_0^L GJ_X\left(\frac{d\varphi}{dx}\right)^2dx. \tag{54}$$

The kinetic energy of the elastic axis with the continuous distribution of mass equals:

$$T=\frac{1}{2}\int_0^L m(x)V_Y^2(x)dx+\frac{1}{2}\int_0^L m(x)V_Z^2(x)dx+\frac{1}{2}\int_0^L I_X(x)\,\Omega_\phi^2(x)\,dx. \tag{55}$$

Substituting Eqs. (54) and (55) into Eqs. (51) yields the equations of motion for elastic blade as follows:

for in-plane bending

$$\int_0^L m(x)\ddot{y}dx+\int_0^L \frac{d^2}{dx^2}\left[EJ_Z\left(\frac{d^2y}{dx^2}\right)\right]dx=\int_0^L\left(F_{Y_{EXT}}(x)-F_{Y_I}(x)\right)dx, \tag{56a}$$

for out-of-plane bending

$$\int_0^L m(x)\ddot{z}dx+\int_0^L \frac{d^2}{dx^2}\left[EJ_Y\left(\frac{d^2z}{dx^2}\right)\right]dx=\int_0^L\left(F_{Z_{EXT}}(x)-F_{Z_I}(x)\right)dx, \tag{56b}$$

and for torsion

$$\int_0^L I_X(x)\ddot{\phi}\,dx+\int_0^L \frac{d}{dx}\left[GJ_X\left(\frac{d\phi}{dx}\right)\right]dx=\int_0^L\left(M_{S_{EXT}}(x)-M_{S_I}(x)\right)dx, \tag{56c}$$

where

$F_{Y_{EXT}}, F_{Z_{EXT}}, M_{S_{EXT}}$ – shearing forces and torsion moment of external blade loading,

$F_{Y_I}, F_{Z_I}, M_{S_I}$ – inertial forces and moment without components $m\ddot{y}, m\ddot{z}, I_X\ddot{\phi}$.

For the case of rotating blade in equation of motion must be considered the stiffening effects of centrifugal forces. The centrifugal forces per unit length that reduce out-of-plane bending moments are equal:

$$p_{Z_\Omega}=\frac{d}{dx}\left(N\frac{dz}{dx}\right), \tag{57a}$$

and in-plane:

$$p_{Y_\Omega} = \frac{d}{dx}\left(N \frac{dy}{dx} \right) - m(x)\omega^2 y, \tag{57b}$$

where

$$N = \int_r^R m(x)\omega^2 x\, dx \tag{57c}$$

the centrifugal force for cross section in distance r from axis of the tail rotor shaft.

Using Eqs. (56) and Eqs. (57) the equations of motion of whirling elastic blade can be written in following form:

$$\int_0^R m(x)\ddot{y}\, dx + \int_0^R \left\{ \frac{d^2}{dx^2}\left[EJ_Z \left(\frac{d^2 y}{dx^2} \right) \right] - \frac{d}{dx}\left(N \frac{dy}{dx} \right) + m(x)\omega^2 y \right\} dx = \int_0^R \left(F_{Y_{EXT}} - F_{Y_I} \right) dx, \tag{58a}$$

$$\int_0^R m(x)\ddot{z}\, dx + \int_0^R \left\{ \frac{d^2}{dx^2}\left[EJ_Y \left(\frac{d^2 z}{dx^2} \right) \right] - \frac{d}{dx}\left(N \frac{dz}{dx} \right) \right\} dx = \int_0^R \left(F_{Z_{EXT}} - F_{Z_I} \right) dx, \tag{58b}$$

$$\int_0^R I_X(x)\ddot{\phi}\, dx + \int_0^R \frac{d}{dx}\left[GJ_X \left(\frac{d\phi}{dx} \right) \right] dx = \int_0^R \left(M_{S_{EXT}} - M_{S_I} \right) dx. \tag{58c}$$

The solution to Eqs. (58) can be obtained using a Galerkin procedure. The deformations of elastic blade axis y, z, φ are assumed as a superposition of modal solution ρ_{i1}, δ_{i2}, η_{i3} of the form:

$$y(x.t) = \sum_{i1=1}^{I1} \rho_{i1}(t) y_{i1}(x), \tag{59a}$$

$$z(x,t) = \sum_{i2=1}^{I2} \delta_{i2}(t) z_{i2}(x), \tag{59b}$$

$$\varphi(x,t) = \sum_{i3=1}^{I3} \eta_{i3}(t) \varphi_{i3}(x), \tag{59c}$$

where

$y_{i1}, z_{i2}, \varphi_{i3}$ – are blade eigen modes for in-plane bending, out-of-plane bending and torsion respectively,

I1, I2, I3 – are numbers of eigen modes for bending and torsion.

Taking into consideration Eqs. (59) the blade motion equations (58) can be transformed to a set of differential equations:

$$\ddot{\rho}_{i1} + \rho_{i1} p_{i1}^2 = Q_{Y_{i1}}, \qquad \text{i1} = 1, \ldots, \text{I1} \tag{60a}$$

$$\ddot{\delta}_{i2} + \delta_{i2} f_{i2}^2 = Q_{Z_{i2}}, \qquad \text{i2} = 1, \ldots, \text{I2} \tag{60b}$$

$$\ddot{\eta}_{i3} + \eta_{i3} \nu_{i3}^2 = Q_{\phi_{i3}}, \qquad \text{i3} = 1, \ldots, \text{I3} \tag{60c}$$

where

p_{i1}, f_{i2}, ν_{i3} are eigen frequencies of the considered modes,

$Q_{Y_{i1}}, Q_{Z_{i2}}, Q_{\varphi_{i3}}$ – are generalized forces.

Replacing the continuous mass distribution by system of lumped masses the generalized forces can be defined in the following way:

$$Q_{Y_{i1}} = \frac{\sum_{j=1}^{J}\left(F_{Y_{EXT}} - F_{Y_B}\right)_j \left(y_{i1}\right)_j}{\sum_{j=1}^{J} m_j \left(y_{i1}\right)_j^2}, \tag{61a}$$

$$Q_{Z_{i2}} = \frac{\sum_{j=1}^{J}\left(F_{Z_{EXT}} - F_{Z_B}\right)_j \left(z_{i2}\right)_j}{\sum_{j=1}^{J} m_j \left(z_{i2}\right)_j^2}, \tag{61b}$$

$$Q_{\phi_{i3}} = \frac{\sum_{j=1}^{J}\left(M_{S_{EXT}} - M_{S_B}\right)_j \left(\phi_{i3}\right)_j}{\sum_{j=1}^{J} I_{Xj} \left(\phi_{i3}\right)_j^2}, \tag{61c}$$

where J – number of lumped masses for the tail rotor blade.

The Runge-Kutta algorithm is used to solve the set of equations (60). Integrating the distribution of forces and moments along the blades makes it possible to calculate the loads of tail rotor hub and shaft.

5. INERTIAL FORCES OF BLADE SEGMENT

Aerodynamic and inertial forces are taken into consideration to define the generalized forces as given in equations (61) for the considered modes of the tail rotor blade. Calculating the inertial forces of blade segments requires defining the acceleration of the lumped mass segments. The position of the lumped mass of i^{th} segment of l^{th} blade given relative to the mass center of helicopter can be defined as follows (Fig. 4):

$$\overline{r}_{M_{li}} = \overline{r}_{tr} + \overline{r}_{Li}, \tag{62}$$

where

$\overline{r}_{tr}$ – position vector of the center of the tail rotor hub relative to the mass center of helicopter,

$\overline{r}_{Li}$ – position vector of lumped mass of the segment blade relative to the center of the tail rotor hub.

The components of position vector $\overline{r}_{Li}$ for lumped mass of the segment blade defined in non rotating coordinate system $O_W X_\psi Y_\psi Z_\psi$ are equal:

$$x_{Li} = x^*_{Li} \cdot \cos\Psi - y^*_{Li} \cdot \sin\Psi, \tag{63a}$$

$$y_{Li} = x^*_{Li} \cdot \sin\Psi + y^*_{Li} \cdot \cos\Psi, \tag{63b}$$

$$z_{Li} = z^*_{Li}. \tag{63c}$$

The components of position vector $\overline{r}^*_{Li} = \left[x^*_{Li}, y^*_{Li}, z^*_{Li}\right]$ of lumped mass given in rotating with blade coordinate system $O_W X_L Y_L X_L$ are following:

$$x^*_{Li} = x_i - e_i\gamma_i - f_i\alpha_i, \tag{64a}$$

$$y^*_{Li} = y_i + e_i - f_i\Phi_i, \tag{64b}$$

$$z^*_{Li} = z_i + e_i\Phi_i + f_i, \tag{64c}$$

where

x_i – position of lumped mass of segment measured along the blade for non-deformed elastic axis,

y_i, z_i, Φ_i – deformations of blade elastic axis: deflection in-plane, deflection out-of-plane and twist,

e_i, f_i – distances defining position of lumped mass of segment relative to non deformed blade elastic axis for in-plane and out-of-plane respectively,

α_i, γ_i – angles of deflection of blade elastic axis out-of-plane and in-plane.

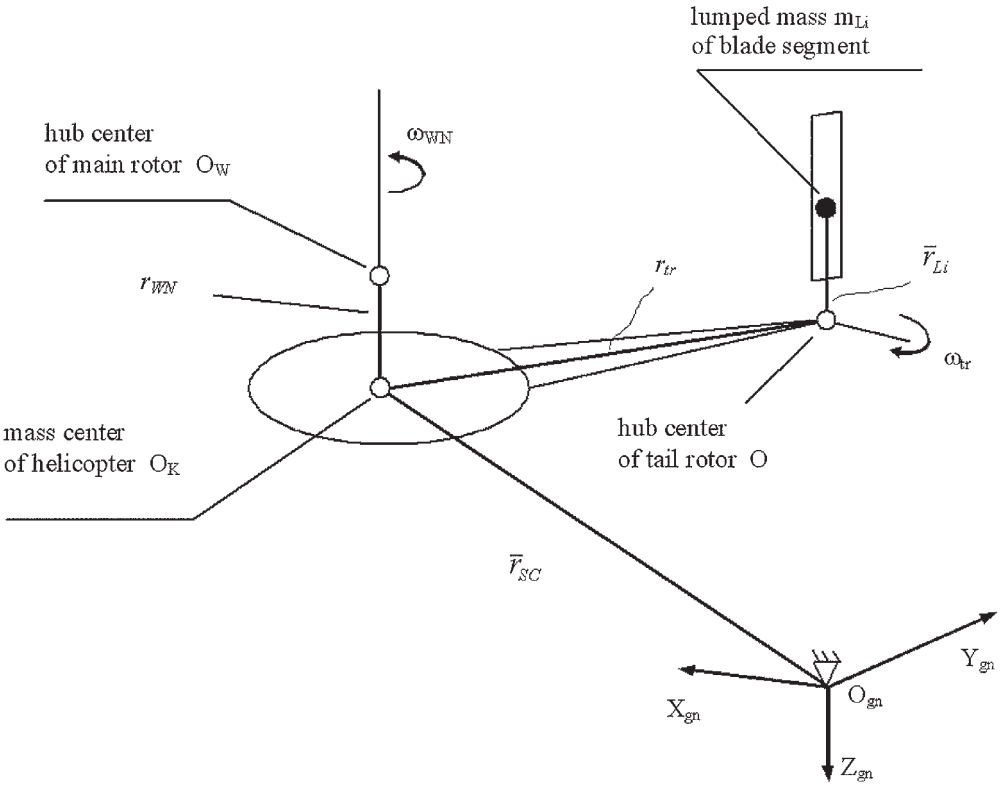

Fig. 4. Position of lumped mass of the tail rotor segment blade

In case of flying helicopter the speed of lumped mass of blade segment can be defined according to following expression:

$$\bar{V}_{M_{Li}} = \bar{V}_{SC} + \bar{\Omega}_k \times \left(\bar{r}_{tr} + \bar{r}_{Li}\right) + \bar{\Omega}_{tr} \times \bar{r}_{Li} + \frac{\delta \bar{r}^*_{Li}}{\delta t}, \tag{65}$$

where

$\bar{\Omega}_k$ – angular speed of helicopter fuselage,

$\bar{\Omega}_{tr} = [0, 0, \omega_{tr}]$ – angular speed of the tail rotor shaft,

$\frac{\delta \bar{r}^*_{Li}}{\delta t}$ – speed vector of lumped mass of blade segment defined in coordination system $O_W X_L Y_L Z_L$ bounded with l^{th} blade, components of speed vector according to equations (64) are equal:

$$\dot{x}^*_{Li} = -e_i \dot{\gamma}_i - f_i \dot{\alpha}_i, \tag{66a}$$

$$\dot{y}^*_{Li} = \dot{y}_i - f_i \dot{\Phi}_i, \tag{66b}$$

$$\dot{z}^*_{Li} = \dot{z}_i + e_i \dot{\Phi}_i. \tag{66c}$$

Differentiating expression (65) the acceleration vector of lumped mass of blade segment is obtained including the effects of fuselage motion as rigid body:

$$\overline{p}_{M_{Li}} = \overline{p}_{SC} + \dot{\overline{\Omega}}_k \times \left[\overline{r}_{tr} + \overline{r}_{Li}\right] + \overline{\Omega}_k \times \overline{\Omega}_k \times \left[\overline{r}_{tr} + \overline{r}_{Li}\right] + 2\overline{\Omega}_k \times \left[\overline{\Omega}_{tr} \times \overline{r}_{Li} + \frac{\delta \overline{r}_{Li}^*}{\delta t}\right] +$$

$$+ 2\overline{\Omega}_{tr} \times \frac{\delta \overline{r}_{Li}^*}{\delta t} + \dot{\overline{\Omega}}_{tr} \times \overline{r}_{Li} + \overline{\Omega}_{tr} \times \overline{\Omega}_{tr} \times \overline{r}_{Li} + \frac{\delta^2 \overline{r}_{Li}^*}{\delta t^2}, \tag{67}$$

where

$\frac{\delta^2 \overline{r}_{Li}^*}{\delta t^2}$ – acceleration vector of lumped mass of blade segment defined in coordination system $O_W X_L\ Y_L\ Z_L$ bounded with l^{th} blade, components of acceleration vector according to equations (66) are equal:

$$\ddot{x}_{Li}^* = -e_i \ddot{\gamma}_i - f_i \ddot{\alpha}_i, \tag{68a}$$

$$\ddot{y}_{Li}^* = \ddot{y}_i - f_i \ddot{\Phi}_i, \tag{68b}$$

$$\ddot{z}_{Li}^* = \ddot{z}_i + e_i \ddot{\Phi}_i . \tag{68c}$$

The equation (67) defines the acceleration of mass segment of the tail rotor blade in any case of helicopter motion.

6. AERODYNAMIC FORCES OF BLADE SEGMENT

Aerodynamic forces acting on blade segment at given its azimuth position on tail rotor disk are calculated using blade element theory. The local angle of attack α depends on instantaneous conditions of airflow of blade profile along rotor radius:

$$\alpha = \varphi - arctg\left(\frac{v_Z}{v_X}\right), \tag{69}$$

v_Z, v_X – components of blade profile airflow: out-of-plane and in-plane of tail rotor disk,

φ – instantaneous pitch angle of tail rotor blade segment.

Variable with time aerodynamic coefficients c_x, c_z, c_m for blade segment are defined taking into consideration unsteady airflow conditions of blade profile. The dynamic effects of blade element airflow are the results due to continuous changes of incidence angle α during whirling the rotor with mutual varying local Ma number and sweep angle Λ of air stream. The dynamic coefficient of lift for the j^{th} segment of the l^{th} blade can be estimated using following expression:

$$\left(C_{ZDYN}\right)_{lj} = \left(\frac{dC_Z}{d\alpha}\right)_{lj} \cdot \left[F \cdot \alpha_{lj} + \left(\frac{k}{2} + G\right) \cdot \frac{d\alpha_{lj}}{d\psi} + 2 \cdot \left(\frac{3}{4} - a\right) \cdot F \cdot k \cdot \frac{d\alpha_{lj}}{d\psi}\right] +$$

$$- \left(\frac{dC_Z}{d\alpha}\right)_{lj} \cdot \left[k^2 \cdot \left(a - \frac{1}{2}\right) \cdot \frac{d^2\Theta_{lj}}{d\psi^2}\right], \tag{70}$$

where

F, G – Theodorsen's functions,

a – blade pitching axis distance to leading edge given in % of chord,

$k = \frac{b \cdot \Omega}{2 \cdot V_{lj}}$ – non-dimensional frequency calculated for each blade segment,

$\Theta(\psi)$ – function of blade pitch angle,

α_{lj} – local attack angle of blade segment.

The static characteristics of the aerodynamic profile can be used to calculate the dynamic angle of incidence introducing the equivalent angle of attack defined following:

$$\left(\alpha_{EQV}\right)_{lj} = \alpha_{lj} - \gamma \cdot \left(\frac{b \cdot \dot{\alpha}_{lj}}{2 \cdot V_{lj}}\right)^{0,5} \cdot sign\left(1, \dot{\alpha}_{lj}\right), \tag{71}$$

where

γ – parameter dependent on kind of the aerodynamic profile and Mach number,

$\dot{\alpha}_{lj} = \frac{d\alpha_{lj}}{d\psi}$ – rate of change the attack angle of blade segment,

$$\dot{\alpha}_{lj}(r_{lj}, \psi) = \frac{\alpha_{lj}(t + \Delta t) - \alpha_{lj}(t)}{\Delta \psi}. \tag{72}$$

Value of aerodynamic coefficients C_z, C_m, C_x and temporary parameters of local flow are determined for the equivalent attack angle α_{EQV} of blade segment. Taking into consideration the static lift characteristic $C_z = f(\alpha)$ the value of critical attack angle α_{cr} is calculated:

for Mach number $M_{lj} < 0.3$ $$\alpha_{cr} = \frac{C_{z\max}}{a_{lj\infty} \cdot \left|\cos \Lambda\right|}, \tag{73a}$$

for Mach number $M_{lj} > 0.3$ $$\alpha_{cr} = \frac{1}{a_{lj\infty} \cdot \left|\cos \Lambda\right|} \cdot \left[C_{z\max} + \frac{\partial C_{z\max}}{\partial M} \cdot (M - 0.3)\right]. \tag{73b}$$

The local value of lift C_z coefficient including the compressibility effects and sweep angle of flow is equal:

for $M_{lj} < M_{cr}$ $$\left(C_z\right)_{lj} = \frac{\alpha_{EQV} \cdot a_{lj\infty}}{\sqrt{1 - M^2}} \cdot \frac{1}{\cos \Lambda_{lj}}, \tag{74a}$$

dla $M_{lj} > M_{cr}$ $$\left(C_z\right)_{lj} = \frac{\alpha_{EQV} \cdot a_{lj\infty}}{\cos \Lambda_{lj}}, \tag{74b}$$

where $a_{lj\infty}$ derivative of lift coefficient C_z due to the attack angle.

The corrected value a_{ljs} of slope angle for the lift characteristic equals:

$$a_{ljs} = \frac{\left(C_z\right)_{lj}}{\left(\alpha_{EQV}\right)_{lj}}, \tag{75}$$

Hence substituting $a_{ljs} = \frac{dC_z}{d\alpha}$ to expression (71) the corrected lift coefficient C_{ZDYN} can be defined.

The coefficient of pitching moment for blade segment is calculated using approximation of airfoil static characteristic:

for $\alpha_{EQV\,lj} < \alpha_{cr\,lj}$ $$C_{mlj} = C_{m0} + a_{1cm} \cdot \alpha_{EQVlj}, \tag{76a}$$

for $\alpha_{EQV\,lj} > \alpha_{cr\,lj}$ $$C_{mlj} = C_{m1} + a_{2cm} \cdot (\alpha_{EQVlj} - \alpha_{crlj}), \tag{76b}$$

where

C_{m0} – pitching moment coefficient of blade segment airfoil for $\alpha = 0$,

C_{m1} – pitching moment coefficient of blade segment airfoil for $\alpha = \alpha_{cr}$,

a_{1cm} – derivative of pitching moment coefficient C_m due to attack angle before the separation of flow,

a_{2cm} – derivative of pitching moment coefficient C_m due to attack angle after the separation of flow.

The drag coefficient for blade segment is defined using following expressions approximating function $C_x(\alpha)$:

for Mach number $M_{lj} < M_{cr}$ $$\left(C_x\right)_{lj} = C_{x0} \cdot \left[1 + \left(\frac{\alpha_{EQV} \cdot a_{lj\infty}}{\sqrt{1 - M^2}}\right)^2 \cdot A_X\right], \tag{77a}$$

and for Mach number $M_{lj} > M_{cr}$ $$\left(C_x\right)_{lj} = C_{x0} \cdot \left[1 + \left(\frac{\alpha_{EQV} \cdot a_{lj\infty}}{\sqrt{1 - M^2}}\right)^2 \cdot A_X\right] + B_X \cdot \left(M_{lj} - M_{krlj}\right)^{DX}, \tag{77b}$$

where

A_X, B_X, D_X – coefficients of function approximating the drag characteristic $C_x = f(\alpha, M)$.

The aerodynamic forces of rotor blade segments are used to calculate the generalized forces for considered modes of blade due to expressions (61).

7. WIND TUNNEL MEASUREMENTS FOR SIMULATION PROGRAM REVISION

The computer program for calculating the loads and deflections of rotor blades was verified using the results of wind tunnel measurements [5] conducted during research concerning influence of airfoil shape faults on the level of rotor loads. The model of main rotor of light helicopter IS-2 mounted at test stand was used to measure rotor hub forces and moments. The rotor radius of model blade was diminished at scale 1:3.23. The input file for computer program includes the mass and stiffness data of model blade and aerodynamic characteristics of the ILHX4A airfoil family [6], [7]. The state of flight parameters and deflections of rotor controls were input in accordance with way of realization the tunnel tests of rotor model.

As function of collective pitch angle the rotor hub load components were calculated for following conditions:

- speed of rotor blade tip v_{tip} = 190 m/s,
- forces and moments of rotor hub were defined at ideal hover with no deflection of swashplate,
- for forward flight condition at speed coefficient μ = 0.132 the decline angle of rotor shaft axis was fixed to α_{shaft} = -5° and swashplate was hold in perpendicular to shaft axis position (no cyclic pitch angle of blades).

At wind tunnel tests the mean values of the rotor hub load components were defined in time slice comprising a few rotor revolutions. The computed results refer to mean values in period of time equals one rotor revolution. The graphs and tables present the comparison of wind tunnel measurements and calculation results:

- for hover conditions Fig. 5, Fig. 6 and table 1,
- for steady level flight Fig. 7÷Fig. 14 and table 2.

For each case at given collective blade pitch angle the rotor thrust was computed in iteration process. The local attack angles of blade sections depend on value of induced velocity in rotor plane which itself is dependent on thrust generated by rotor. The agreement between measurements and calculations for rotor thrust as a function of collective pitch angle is shown in Fig. 5 and Fig. 7. For the rotor shaft torsion moment the calculations give results of lower level than measurements, see Fig. 6 and Fig. 12. At hover the greater differences appeared for low blade pitch angles and at level flight condition the differences between tests and calculations arose for higher range of the pitch angles. The differences between approximation of airfoil aerodynamic data used for calculation and real characteristics of the rotor blade model tested in wind tunnel are probable reason for different values of computed and measured rotor thrust and rotor torque moment. This effect can be found as result of higher level of drag coefficient for model blade due to lower Reynolds number or less geometry accuracy of model airfoil in comparison to the pattern airfoil section used to define aerodynamic characteristics. The measurement conducted for

sector of full scale blade of helicopter IS-2 main rotor confirmed the higher level of drag coefficient related to the characteristics of the pattern airfoil. Additional calculations of the hub forces and moments were conducted for increased to $c_{x0} = 0.009$ drag coefficient instead $c_{x0} = 0.007$. For level flight conditions the computed results at higher blade drag show better accordance to tests for mean value of rotor hub longitudinal force (Fig. 8 and Fig. 13) and for mean value of the rotor shaft torque moment (Fig. 12 and Fig. 14).

For hub of rotor model the comparison of measured and calculated forces and moments is given in following tables.

Table 1. Comparison of measured and calculated the hub loads of rotor model at hover condition

Collective pitch at R_{07} [deg]	**measurement**		**calculation**	
	T_z [N]	**M_z [Nm]**	**T_z [N]**	**M_z [Nm]**
-0.19	2.9	16.9	0.93	9.59
0.9	42.9	17.2	37.80	9.90
1.87	99.4	18.5	91.61	11.06
3.0	166.7	20.5	165.46	13.44
3.86	219.8	22.5	227.34	16.01
4.81	288.0	25.6	299.97	19.49
5.81	362.5	29.7	380.52	23.95
6.78	435.0	34.5	462.10	28.96
7.76	513.0	40.3	547.65	34.65
8.76	596.1	47.0	637.91	41.06
9.80	677.4	54.9	734.64	48.33
10.76	757.4	62.6	826.15	55.48
11.66	834.7	71.3	913.65	62.45
12.70	922.3	80.9	1016.27	70.82

Table 2.a. Comparison of mean values of rotor hub forces at level flight condition $\mu = 0.132$

Collective pitch at R_{07} [deg]	**measurement**			**calculation**			
	T_z [N]	**H [N]**	**S [N]**	**T_z [N]**	**H [N]**	**S [N]**	**H [N] $cx = .009$**
2.30	127.0	-11.6	-1.3	150.09	-4.96	-1.44	-13.38
4.31	330.1	-15.2	-1.0	344.88	-7.21	-0.97	-15.91
6.03	525.7	-22.6	-1.9	514.84	-10.09	-0.59	-18.86
8.09	721.8	-36.3	-3.7	722.76	-14.78	-0.75	-24.71
9.08	808.0	-42.7	-3.4	824.28	-19.92	0.97	-25.77
10.02	901.3	-51.8	-3.8	921.33	-21.31	0.86	-30.09
11.06	988.3	-63.0	-6.0	1028.69	-27.88	3.60	-35.40

T_z – rotor thrust,
H – rotor longitudinal force (+) forward,
S – rotor side force (+) in direction of rotor disk azimuth 90°,
$Hcx009$ – longitudinal force for increased drag coefficient of blade airfoil.

Table 2.b. Comparison of mean values of rotor hub moments at level flight condition $\mu = 0.132$

Collective pitch at R_{07} [deg]	measurement			calculation			
	M_x [Nm]	M_y [Nm]	M_z [Nm]	M_x [Nm]	M_y [Nm]	M_z [Nm]	M_z [Nm] cx = .009
2.30	1.4	1.5	18.9	0.98	-0.92	11.92	16.38
4.31	2.0	-1.4	23.8	0.30	-2.98	16.50	21.14
6.03	1.4	-3.8	30.0	-0.34	-4.79	21.69	26.52
8.09	0.6	-6.0	40.2	-1.13	-7.09	29.21	34.52
9.08	0.0	-7.1	45.9	-1.56	-8.24	33.20	38.80
10.02	-0.7	-8.2	51.1	-2.00	-9.37	37.33	43.08
11.06	-1.5	-9.3	58.6	-2.51	-10.65	41.98	47.97

M_x – rotor hub rolling moment (+) rotor disk down at azimuth 270°,
M_y – rotor hub pitching moment (+) rotor disk down at azimuth 180° – diving,
M_z – rotor shaft torque moment,
$M_z cx009$ – rotor shaft torque moment for increased drag coefficient of blade airfoil.

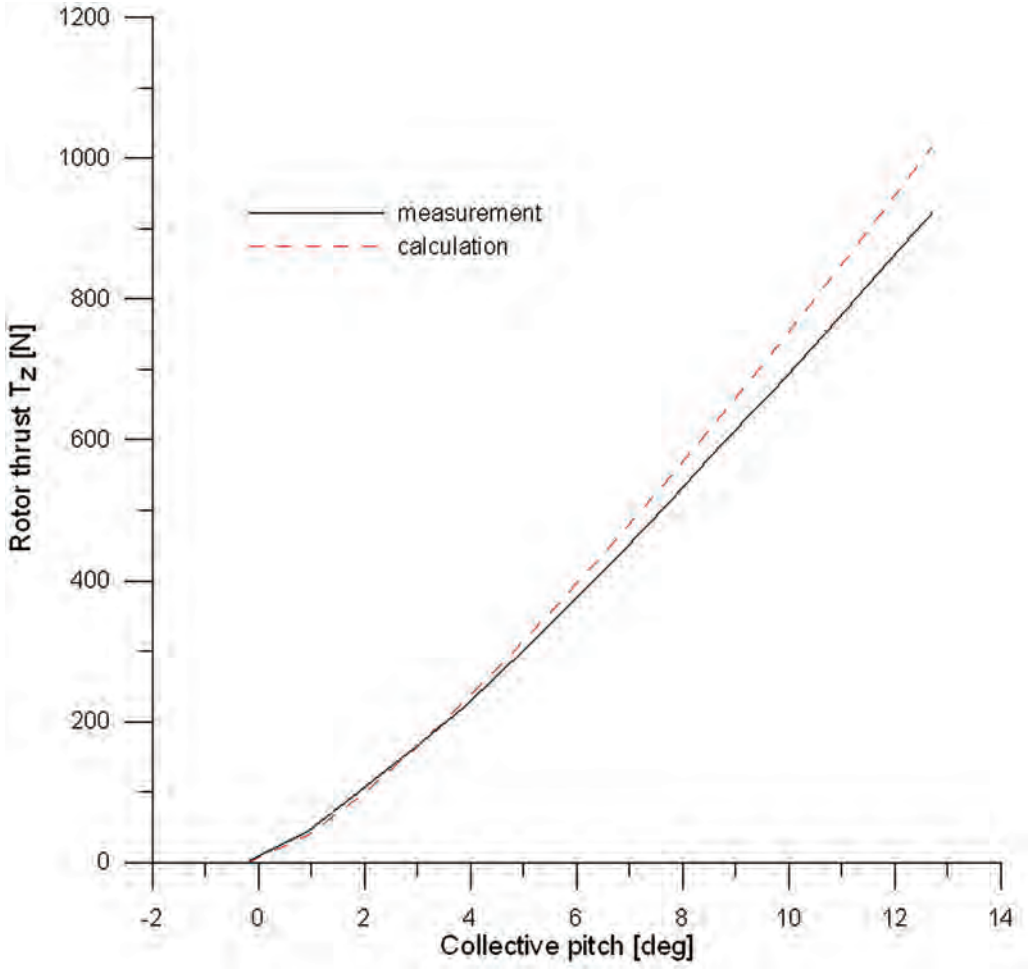

Fig. 5. Changes of thrust of main rotor model of IS-2 helicopter due to blade collective pitch in hover conditions. Comparison of wind tunnel measurements and results of calculation

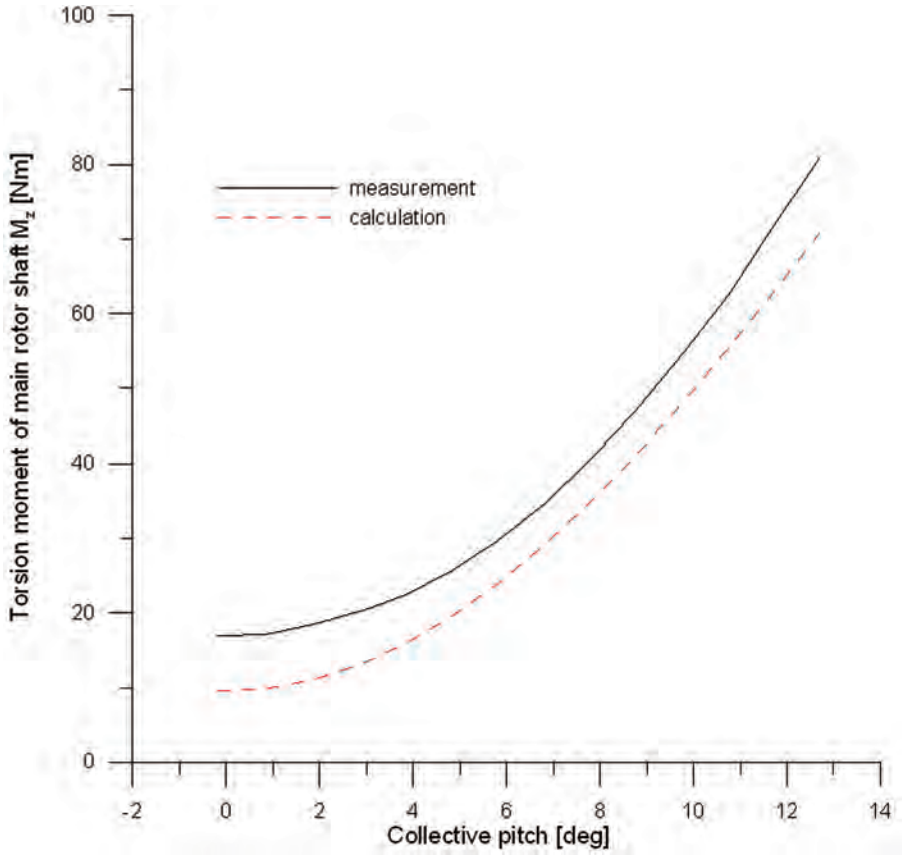

Fig. 6. Changes of torsion moment of main rotor model of IS-2 helicopter due to blade collective pitch in hover conditions. Comparison of wind tunnel measurements and results of calculation

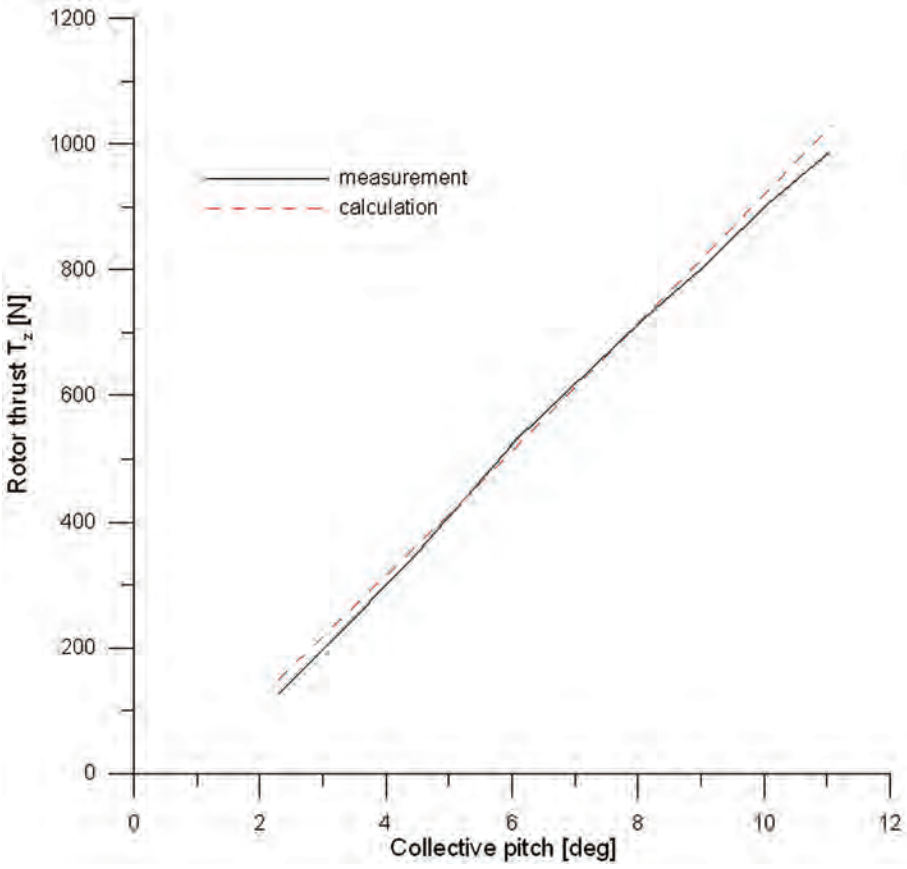

Fig. 7. Changes of thrust of main rotor model of IS-2 helicopter due to blade collective pitch in level flight conditions with speed V = 25.08 m/s (μ = 0.132). Comparison of wind tunnel measurements and results of calculation

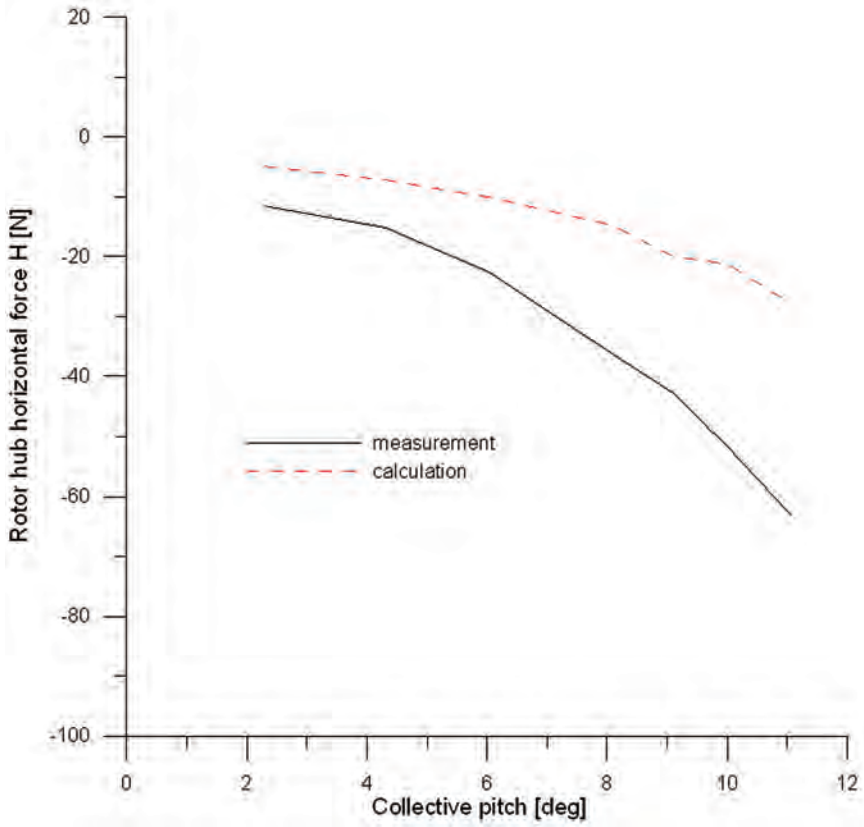

Fig. 8. Changes of hub horizontal force of main rotor model of IS-2 helicopter due to blade collective pitch in level flight conditions with speed V = 25.08 m/s (μ = 0.132).
Comparison of wind tunnel measurements and results of calculation, (-) backward

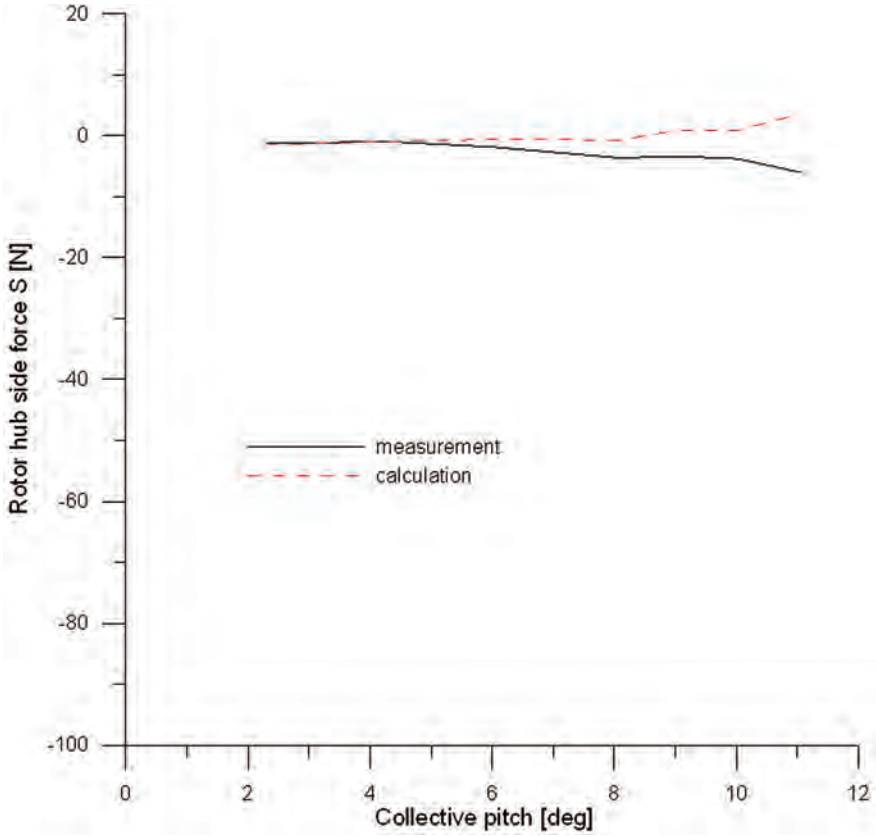

Fig. 9. Changes of hub side force of main rotor model of IS-2 helicopter due to blade collective pitch in level flight conditions with speed V = 25.08 m/s (μ = 0.132).
Comparison of wind tunnel measurements and results of calculation, (+) toward azimuth 90°

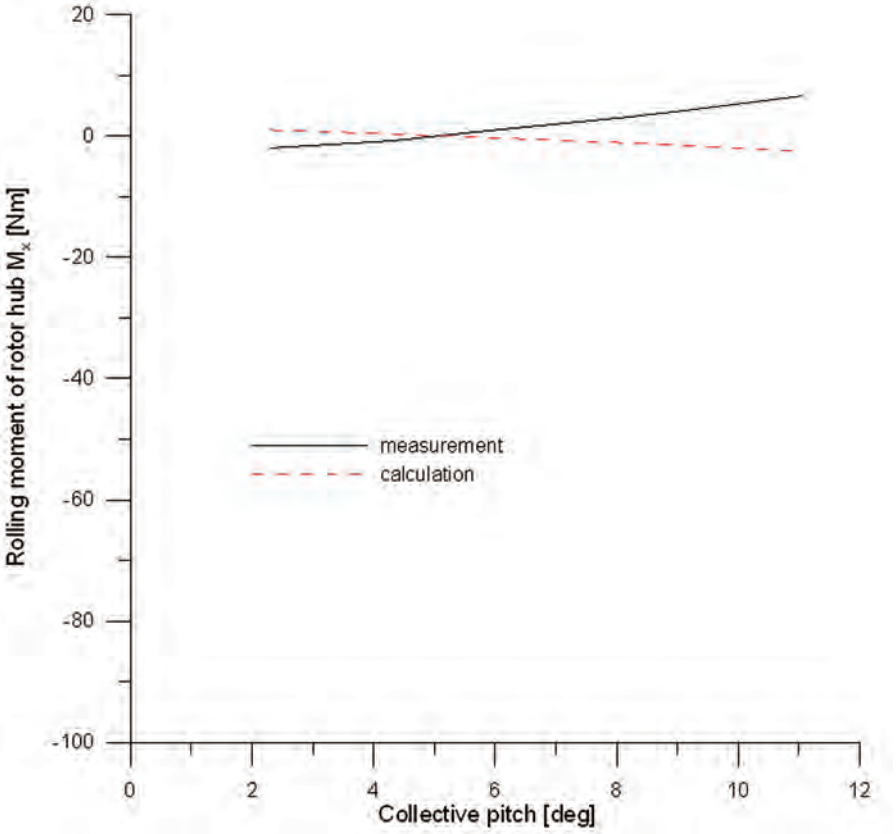

Fig. 10. Changes of hub rolling moment of main rotor model of IS-2 helicopter due to blade collective pitch in level flight conditions with speed V = 25.08 m/s (μ = 0.132). Comparison of wind tunnel measurements and results of calculation

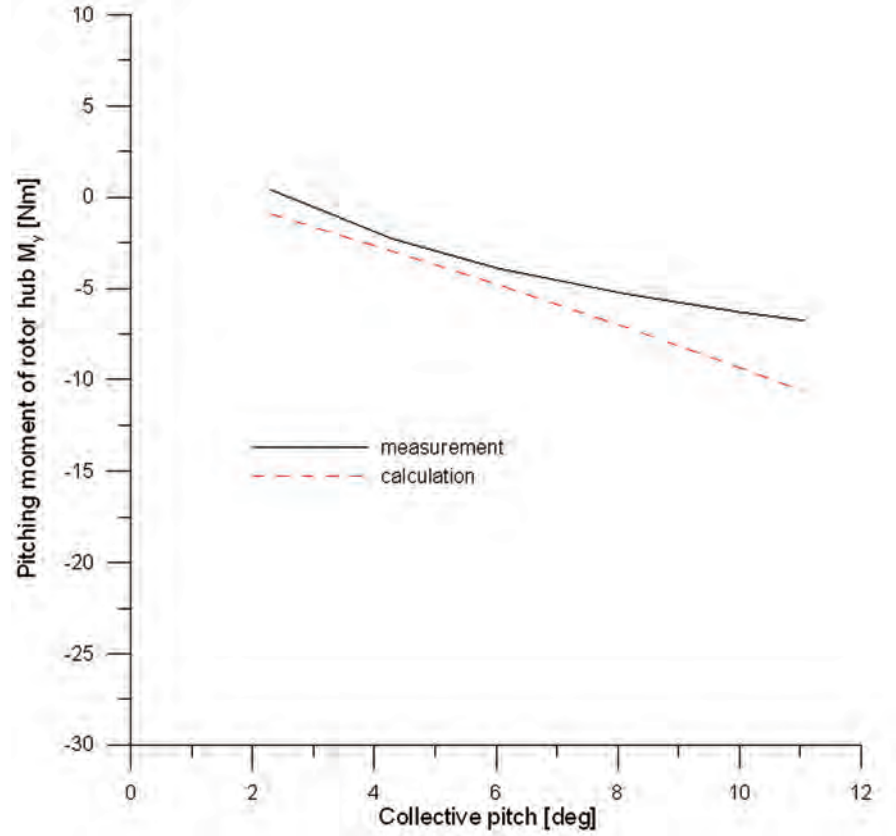

Fig. 11. Changes of hub pitching moment of main rotor model of IS-2 helicopter due to blade collective pitch in level flight conditions with speed V = 25.08 m/s (μ = 0.132). Comparison of wind tunnel measurements and results of calculation, (+) diving

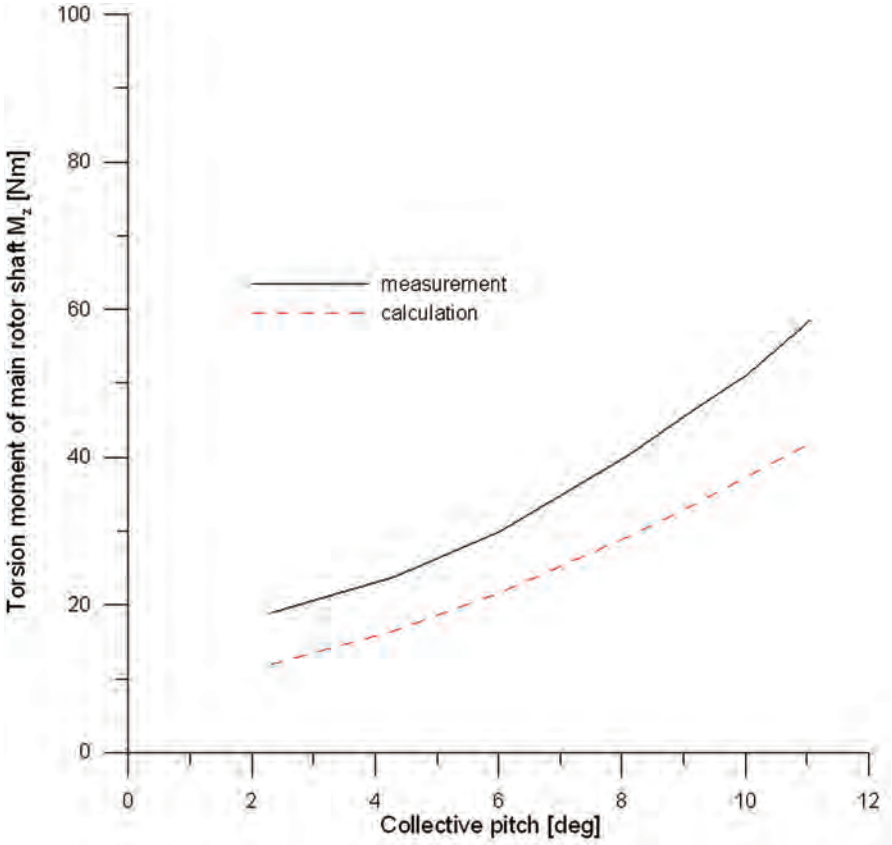

Fig. 12. Changes of shaft torsion moment of main rotor model of IS-2 helicopter due to blade collective pitch in level flight conditions with speed V = 25.08 m/s (μ = 0.132). Comparison of wind tunnel measurements and results of calculation

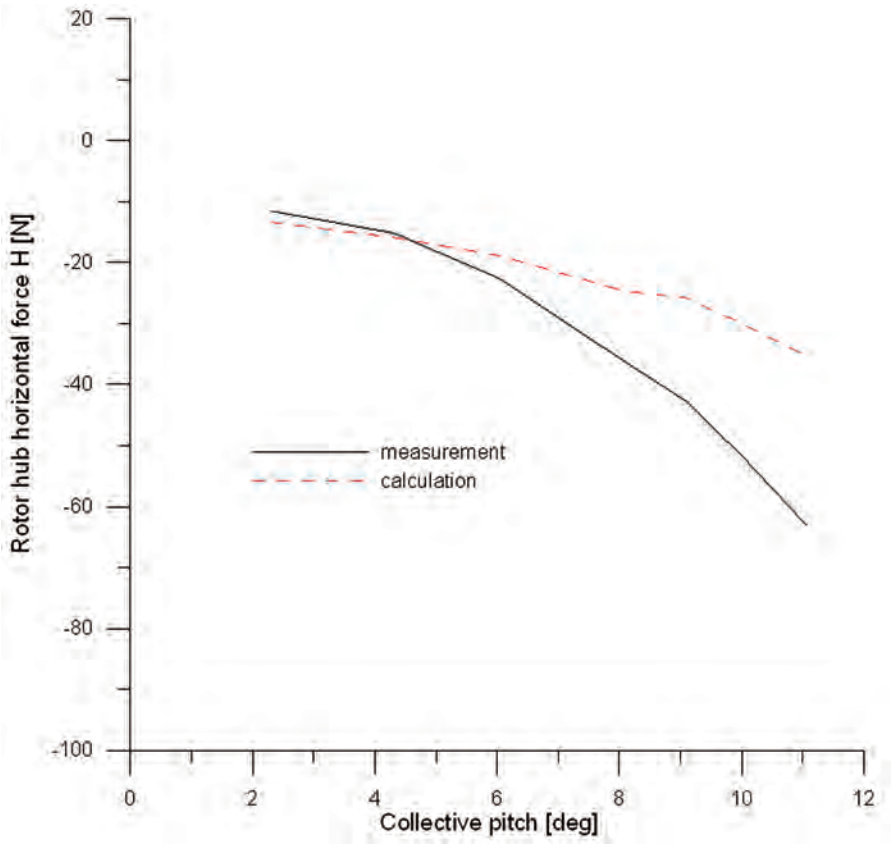

Fig. 13. Changes of hub horizontal force of main rotor model of IS-2 helicopter due to blade collective pitch in level flight conditions with speed V = 25.08 m/s (μ = 0.132). Comparison of wind tunnel measurements and results of calculation for increased airfoil drag coefficient $cx_0 = 0.009$

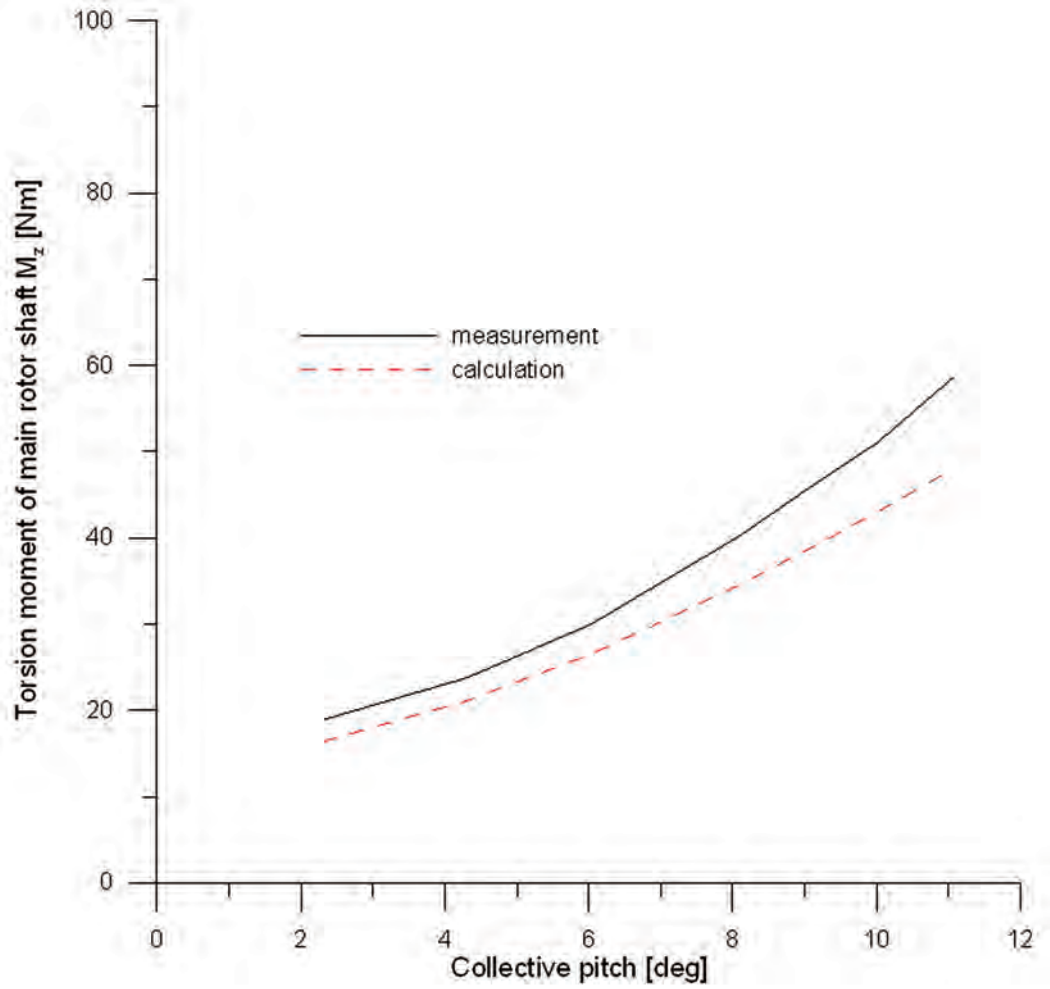

Fig. 14. Changes shaft torsion moment of main rotor model of IS-2 helicopter due to blade collective pitch in level flight conditions with speed V=25.08 m/s (μ=0.132). Comparison of wind tunnel measurements and results of calculation for increased airfoil drag coefficient cx_0=0.009

8. TAIL ROTOR IN YAWING MANEUVER

Assuming the rotation of the stiff fuselage around the central axis which coincides with shaft axis of main rotor the motion of yawing helicopter is considered. The blades of tail rotor are modeled by deformable elastic axes with attached lumped masses. The distribution of mass and stiffness characteristics vary along tail rotor radius.

Determining the equation of motion of helicopter fuselage additional conditions are assumed:

- the mass centre of helicopter during yawing can stay in place or move along the straight line without linear acceleration;
- rotating speed of main rotor and tail rotor in yawing are constant;
- control pitch angle of tail rotor blades as well the airflow changes of fin and blade sections influence only on fuselage rotating motion around axis of the main rotor shaft;
- the influence of side wind gust on flow conditions of tail rotor blades is changing due to increasing fuselage yaw.

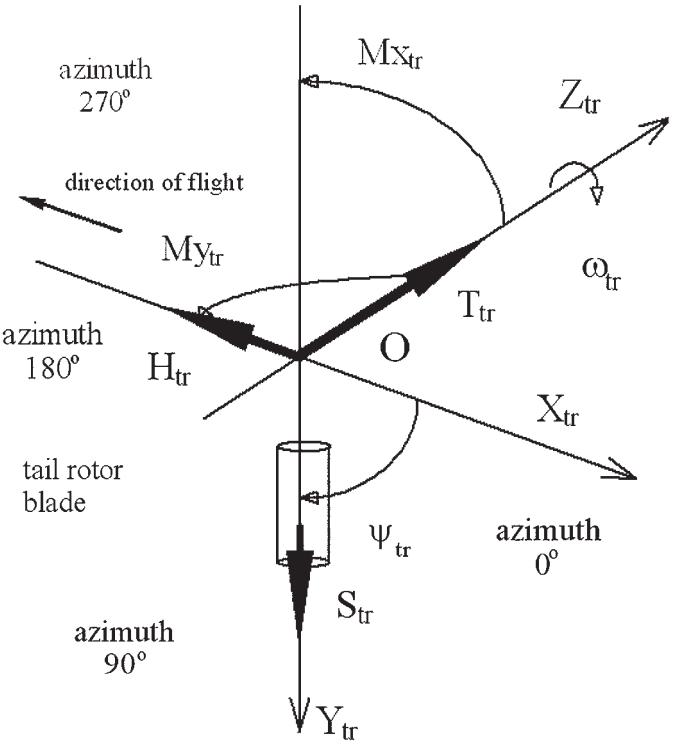

Fig. 15. Scheme of the tail rotor load components in non-rotating coordination system O X_{tr} Y_{tr} Z_{tr} attached at intersection point of tail rotor shaft axis and tail rotor in-plane

The simplified equation of motion of helicopter fuselage during directional maneuver can be written as follows:

$$I\ddot{\beta}_f = M_{mr} + M_f + T_{tr} \times L_{tr} + P_{bv} \times L_{bv} + M_{ytr}, \tag{78}$$

where

I – fuselage second mass moment of inertia relative to axis of the main rotor shaft,
M_{mr} – torque moment of the main rotor,
$M_f(\beta_f)$ – aerodynamic yawing moment for fuselage without fin,
$T_{tr}(\beta_f, \varphi)$ – tail rotor thrust,
$P_{bv}(\beta_f)$ – side component of the fin lift and drag forces,
$M_{ytr}(\beta_f)$ – tail rotor hub moment acts on fuselage as yawing moment (Fig. 15),
β_f – yaw angle of helicopter fuselage,
φ – pitch angle of tail rotor blade.

The equation of fuselage motion (78) is solved for time interval equal few seconds. At this time the tail rotor can accomplish a few hundred revolutions. Time step for solution the equation of fuselage motion is assumed to be equal the period of revolution of tail rotor around its shaft axis. For solution step time the forces and moments in equation (78) are treated as constant. The tail rotor thrust T_{tr} and yawing moment of tail rotor hub M_{ytr} are equal the mean values of run-time during one revolution of the tail rotor.

In course of tail rotor revolution instantaneous values of thrust, yawing moment and other components of tail rotor hub loads are computed in procedure with time step equivalent the angular change $\Delta\psi = 5°$ of blade position on tail rotor disk. The tail rotor blade is modeled by deformable structure consisting of elastic axis with set of lumped masses. The solution of equation of tail rotor blade motion includes the influence of bending and torsion deformation of elastic axis, in-plane and out-of-plane stiffness of hub arm and stiffness of pitch control link. The equations of blade motion are solved using the Runge-Kutta algorithm. In accordance to Galerkin procedure the blade deformations are assumed as a superposition of time dependent components representing the each taken into account eigen mode of the tail rotor blade.

The simulation investigation of the tail rotor work condition in directional maneuver was conducted using data of light helicopter IS-2 [8], [9] with fourbladed tail rotor [10].

The calculations of tail rotor loads were performed for rough blade pitch control in hover, for wind gusts towards the tail rotor disk without pilot reaction and for rough blade pitch control in level flight condition:

- turn in hover, rough control with initial increase of tail rotor thrust, in case of IS-2 helicopter initial turn to the left (Fig. 16÷22);
- turn in hover, brutal control and horizontal wind gust speed V_{gust} = 9 m/s in direction coincident with induced speed of tail rotor, for IS-2 helicopter from right to the left side of fuselage (Fig. 23÷28);
- turn in hover with rough control and horizontal wind gust speed V_{gust} = -9 m/s in direction opposite to induced speed of tail rotor, for IS-2 helicopter from left to the right side of fuselage (Fig. 29÷35);
- wind gust V_{gust} = 9 m/s without pilot reaction (Fig. 36÷41);
- wind gust V_{gust} = -9 m/s without pilot reaction (Fig. 42÷47);
- rough control of tail rotor blade pitch in the level flight with speed V = 191 km/h (Fig. 48÷56).

The brutal control of the tail rotor blade pitch means rough deflection of pedals from position according equilibrium state to the boundary position and next pedals returning after the yaw angle of fuselage has overrun assumed limit value (β_{limit} = 45° in hover and β_{limit} = 15° in level flight). In simulation program the deflection of pedals is represented as the function of changing the tail rotor pitch angle. The full motion of pedals is assumed to be done during time of 1÷2 second, what corresponds the angular speed of blade pitch motion equal 15÷30 deg/s. The range of tail rotor blade pitch between the limits comprises from -8° to 20°.

In Fig. 16 are shown the control function of tail rotor blade pitch and reaction of helicopter in time of maneuver simulation according over 100 revolutions of tail rotor shaft. In simulation after the sixth revolution of the tail rotor shaft the blade pitch began to rise increasing tail rotor thrust T_{tr} (Fig. 18) and fuselage turn to the left. Arising blade pitch was continued up to maximum pitch angle φ_{tr} = 20°. The tail rotor blades were kept in that position to the moment when fuselage yaw angle achieved limit value β_{limit} = 45°. At the next time step of simulation the blade pitch was diminished. During directional maneuver the angular speed and acceleration of fuselage (Fig. 17), tail rotor thrust (Fig. 18) and its torque moment (Fig. 21) were changing at quick rate. According to variable load level of tail rotor the changing twist at blade tip can be watched in Fig. 20.

During maneuver the stall effects appeared on the blade sections of the tail rotor what caused the torque moment increase with simultaneous decreasing of the tail rotor thrust. In Fig. 19 is shown the runtime of difference of the stall and local attack angles at blade tip of tail rotor. Between the 10th and 60th shaft revolution the blade tip section was in stall flow conditions. The distribution of stall region at tail rotor disk for 25th shaft revolution is shown in Fig. 22 as map graph of difference of the stall and local attack angles. The stall region is large and covers the part of blade at all azimuth positions on the rotor disk. The boundary of stall zone, where the difference of the stall and local attack angle is equal zero, takes the circular shape and is central located relative axis of tail rotor shaft.

The influence of side wind on helicopter turn in hover can be noticed comparing the runtime of yawing angle in Fig. 23 and Fig. 29. The wind gust was introduced to simulation during the 10th tail rotor revolution. In case of gust direction coincident with the tail rotor induced speed the additional flow through the rotor disk reduces the attack angle of blade sections what causes less thrust (Fig. 25) and lower angular speed of fuselage. In that condition The wind gust helps to stop yawing motion of fuselage. The maximum fuselage yaw angle reached 100° in presence of wind while without gust the maximum angle was 120°. Reduction of the blade stall region on the rotor disk was the additional effect of gust. The different effects occur in case of wind gust opposite to tail rotor induced speed.

Increased blade attach angles generate more thrust, but during maneuver is created large stall region (Fig. 32). For the 40th tail rotor revolution the map graph of differences of stall and local attack angles shows the stall border of elliptic shape and non-central located relative to shaft axis. Passing through stall borders generates high level oscillating loads and large twist deflections of blade (Fig. 33).

In Fig. 36÷47 are presented the results of simulation of helicopter yawing motion in case of side wind gust without the pilot reaction. The stall region doesn't exist at blade sections for both cases of wind direction relative to induced speed. The fuselage yaw angles reach the limit value $\beta_{limit} = 45°$ in time of 1÷1.5 second. In hover in presence of obstacles due to quick displacement of tail rotor in helicopter turn the enlarged safety margins must be considered.

In Fig. 48÷56 is shown the simulation of directional maneuver in level flight with high speed. In the level flight conditions the torque moment of the main rotor can be partly balanced by lift force of fin so the tail rotor blades can work at lower pitch angle. In the maneuver with rapid increase of tail rotor blade pitch the limit of helicopter sideslip angle $\beta_{limit} = 15°$ is reached in about 1 second. During maneuver the stall region on tail rotor disk appeared at the 30th revolution and is kept up to 80th tail rotor revolution (Fig. 51). In comparison to hover different shape of stall region is shown in Fig. 54÷56 presenting for chosen tail rotor revolutions the map graphs of differences between stall angle and local attack angle of blade sections on tail rotor disk. At the initial phase of maneuver, solution for the 25th revolution, there is no stall on the tail rotor. In course of maneuver due to increasing blade pitch and flow through rotor disk the stall region appears. In Fig. 55 the map graph presents results for the 60th tail rotor revolution, when local attach angles are greater than stall angles for blade position from azimuth less 90° to azimuth over 180°. Passing the stall borders generates large blade loads (Fig. 52). In map graph for the 81st revolution (Fig. 56) one can see that in phase of low blade pitch despite lack of stall region the isolines of differences between stall and local attack angle are being kept in oscillating shape.

The results of simulation show the possibility of stall phenomenon occurrence at the tail rotor blades during directional maneuver of helicopter. The large stall region can decrease the aerodynamic efficiency of tail rotor. The size of stall region is connected with rate of change the blade pitch as well the occurrence and direction of side wind gust.

9. CONCLUSIONS

The simulation calculations concerning the work of tail rotor at direction maneuver of helicopter in hover and level flight condition were conducted.

The occurrence of large stall region at tail rotor blades, decreasing its aerodynamic efficiency, is connected with rate of blade pitch control as well with direction and speed of wind gust.

In case of rough control the stall phenomenon can appear in time about 1 second.

Compound and quickly changing the flow conditions of tail rotor make difficult to apply correct rate of blade pitch control for high maneuverability with preserving proper safety margins.

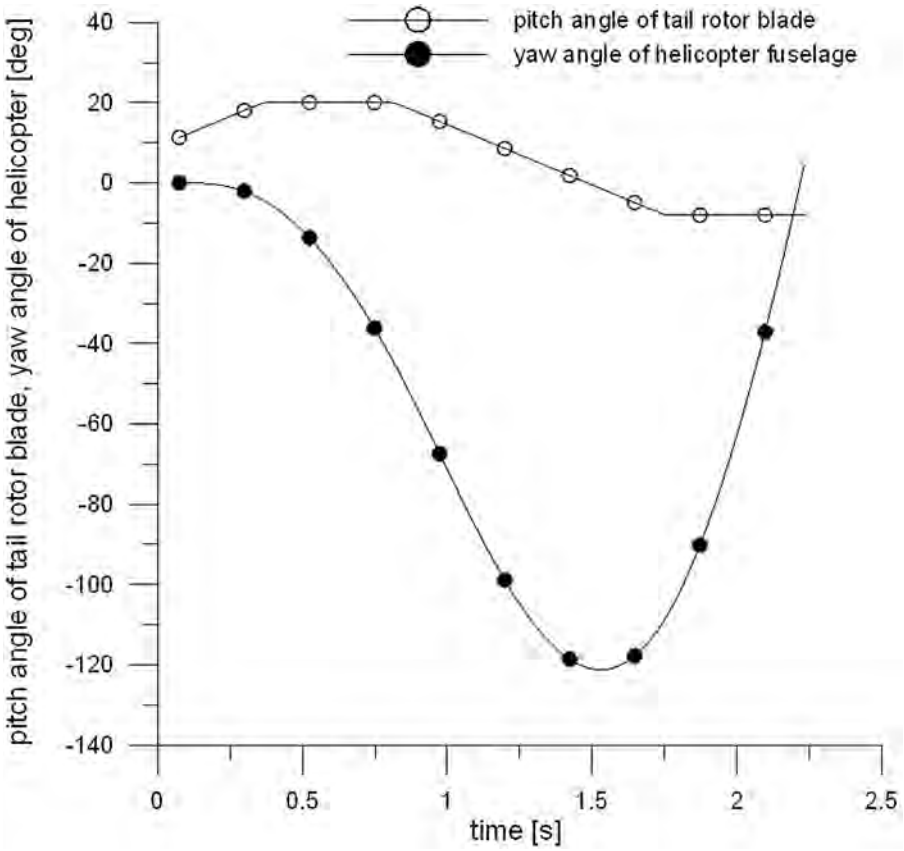

Fig. 16. Function of rough control of pitch angle of tail rotor blade and yaw angle of helicopter in directional maneuver in hover.
Initially the blade pitch was increased, yaw angle (-) for fuselage nose turn to the left

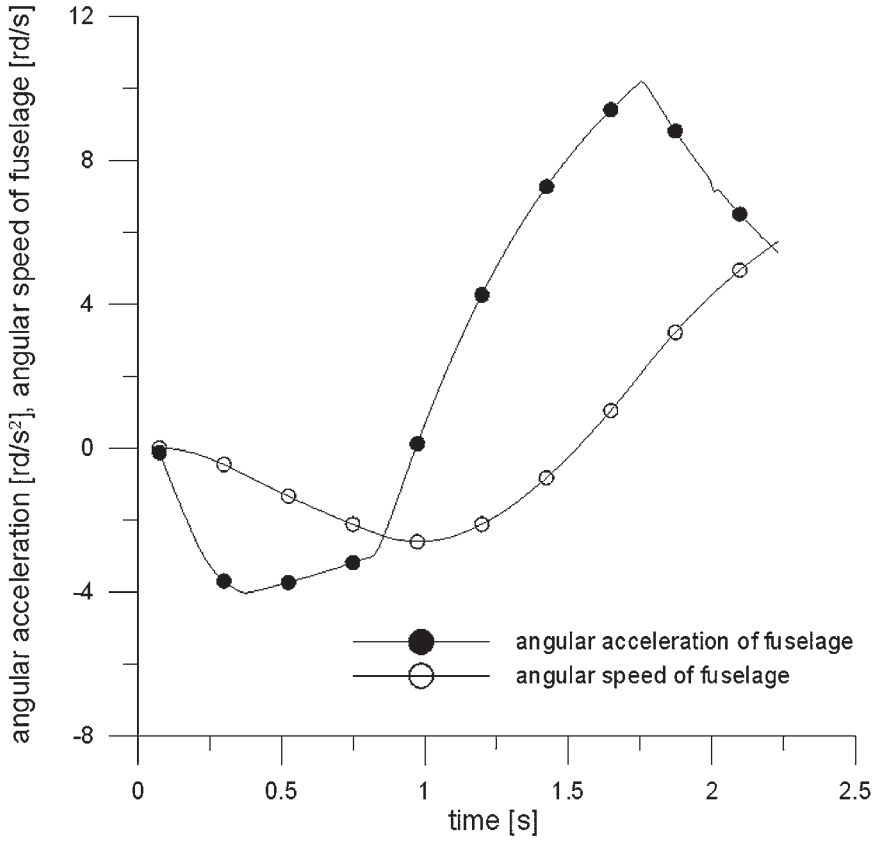

Fig. 17. Angular speed and acceleration of helicopter yawing with rough control of tail rotor blade pitch in directional maneuver in hover. Initially the blade pitch was increased, angular speed and acceleration (-) for fuselage nose turn to the left

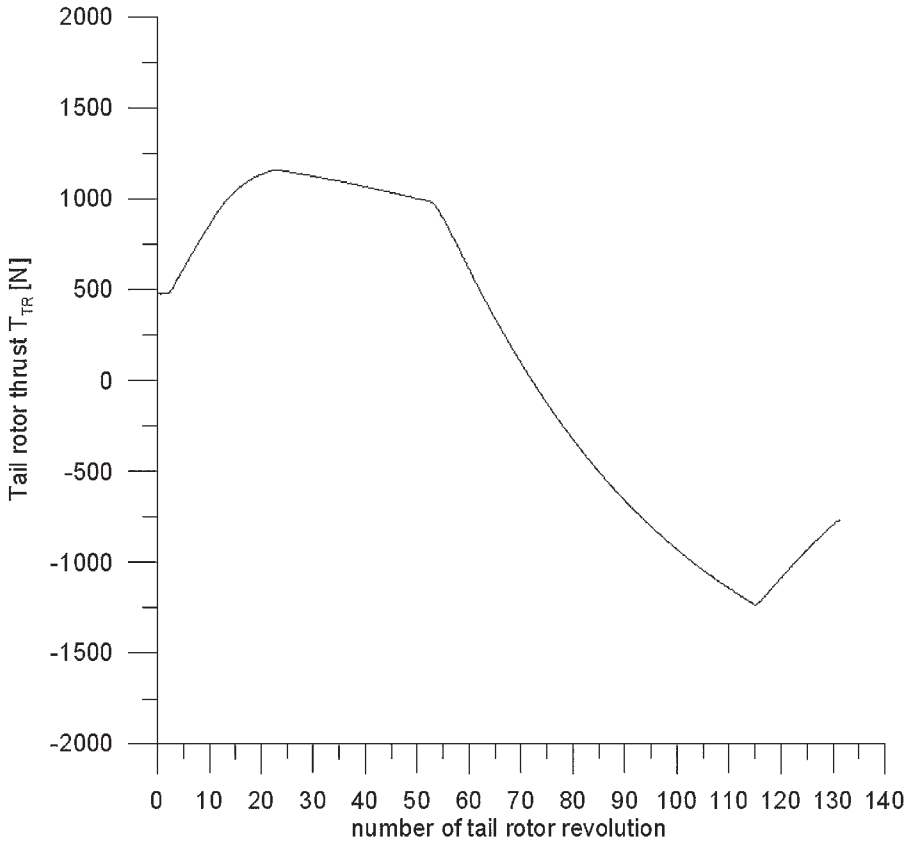

Fig. 18. Tail rotor thrust in directional maneuver in hover. Initially the blade pitch was increased, (+) for tail rotor thrust toward azimuth 90° of the main rotor disk

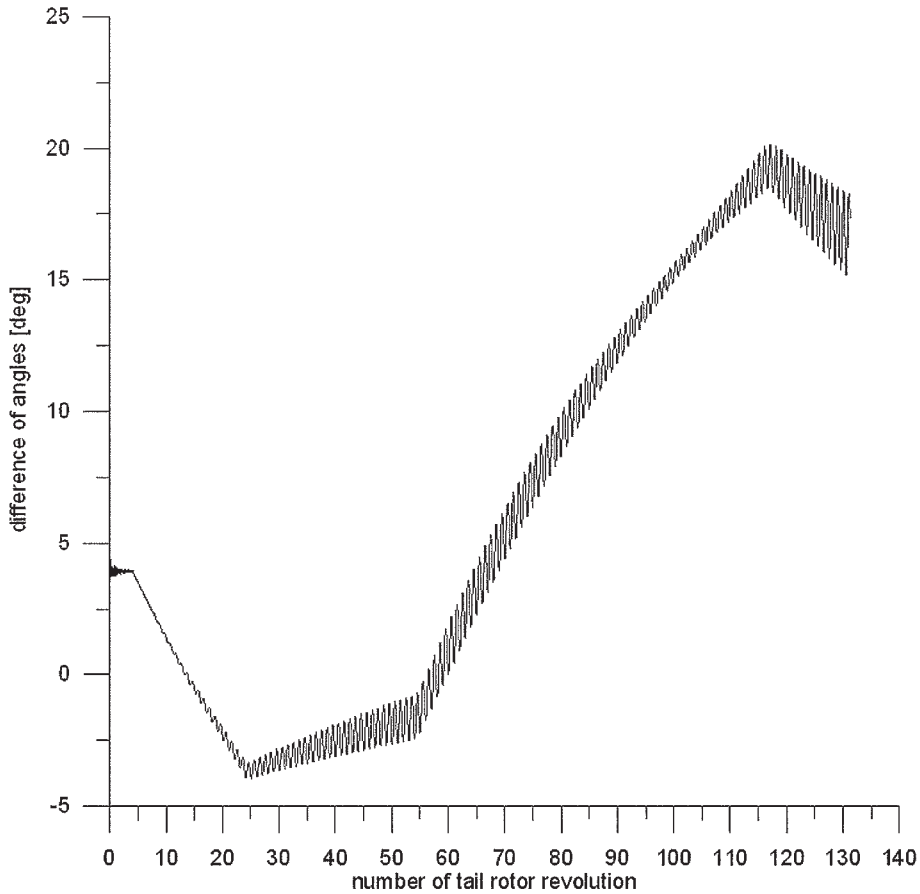

Fig. 19. Differences between stall and local attack angles at blade tip of tail rotor during directional maneuver in hover with rough blade pitch control. Initially the blade pitch was increased

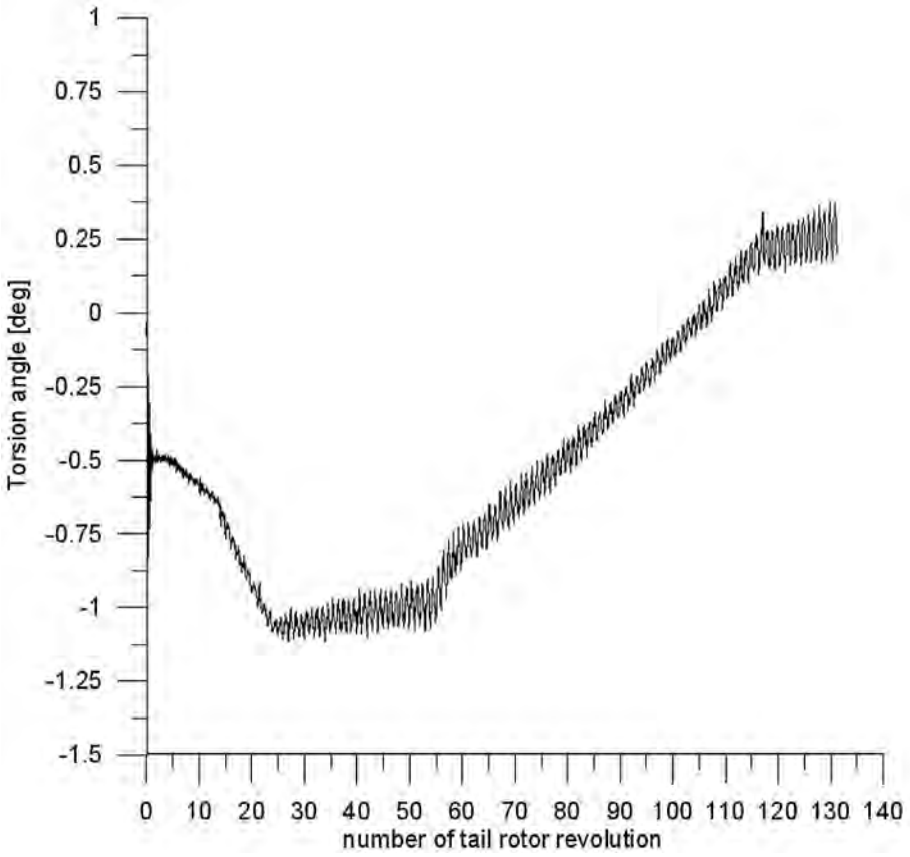

Fig. 20. Torsion angle of blade tip of tail rotor during directional maneuver in hover. Rough blade pitch control. Initially the blade pitch was increased

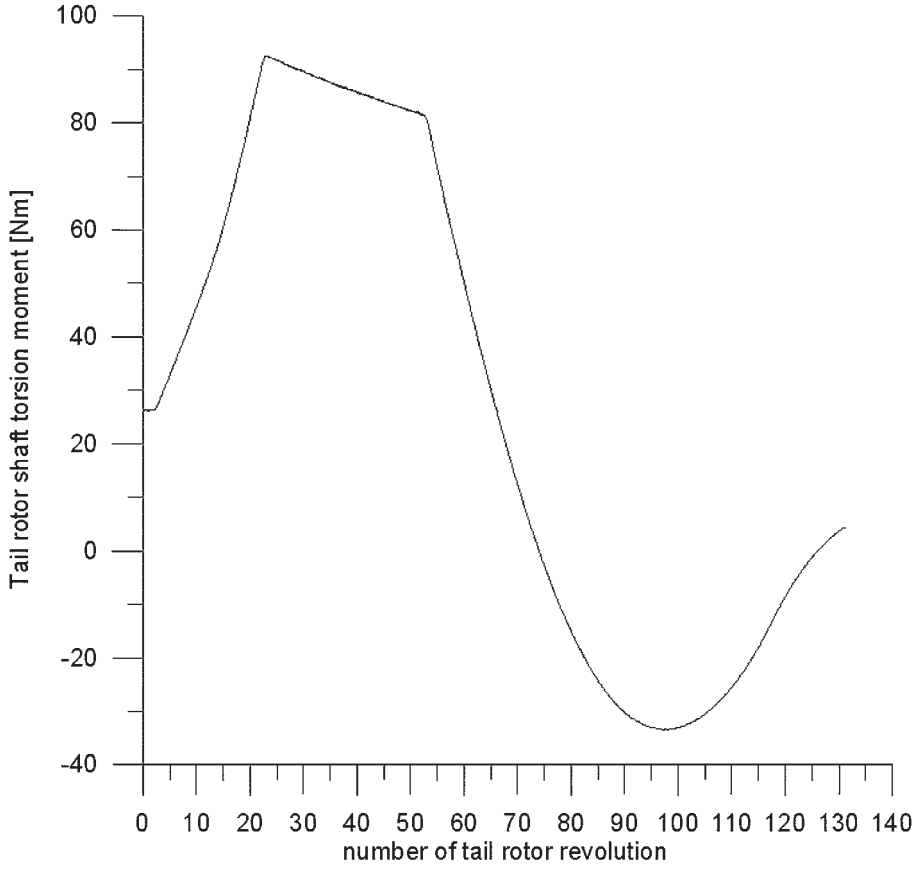

Fig. 21. Torsion moment of tail rotor shaft during directional maneuver in hover with rough blade pitch control. Initially the blade pitch was increased. Negative value of moment for autorotation condition of the tail rotor

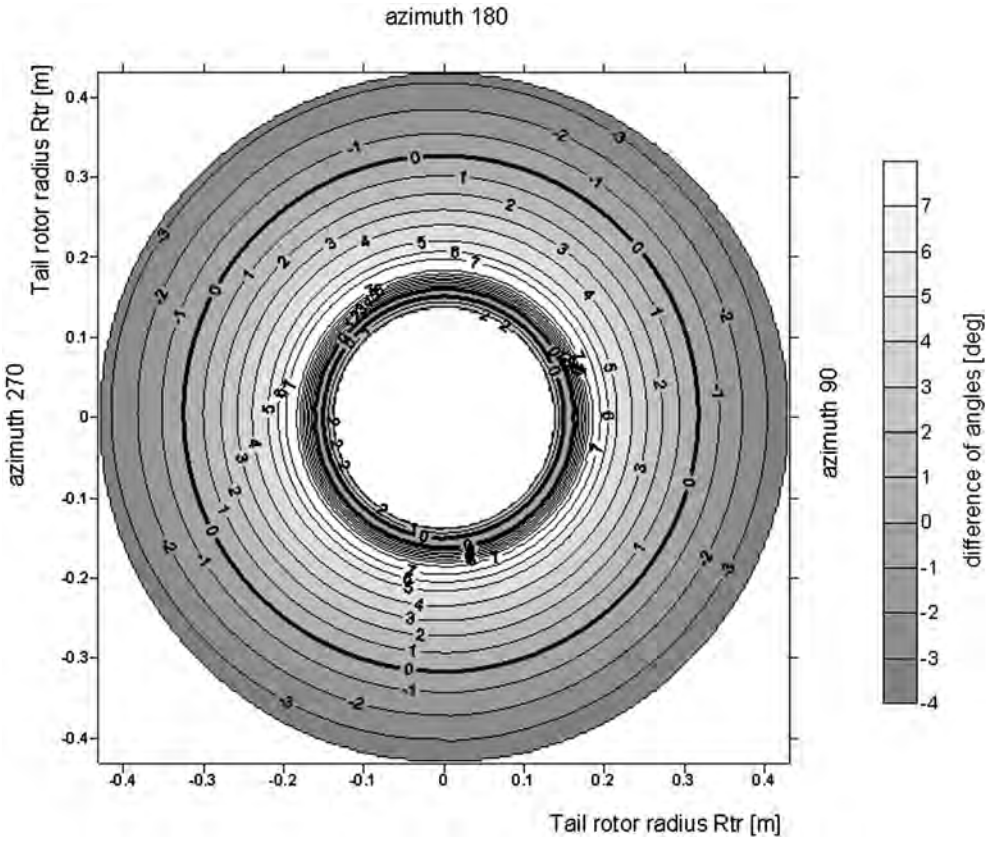

Fig. 22. The differences of stall and local attack angle at the tail rotor disk in directional maneuver with rough blade pitch control. Map for 25th rotor revolution at initial phase of maneuver. The blade tip in stall condition at all perimeter of the tail rotor disk

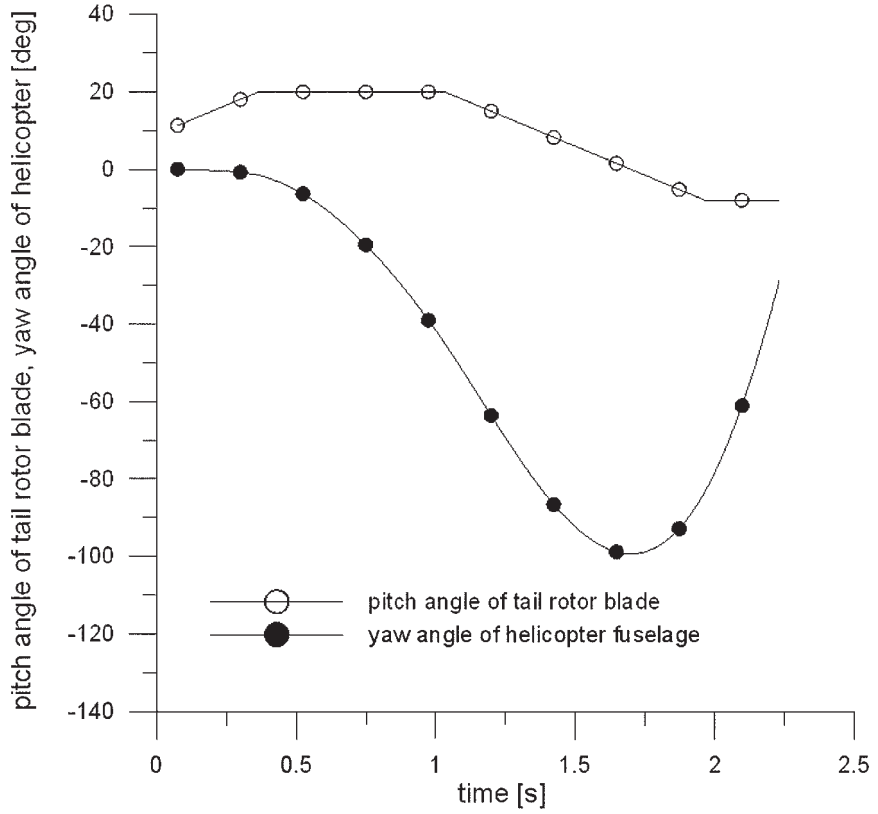

Fig. 23. Function of rough control of pitch angle of tail rotor blade and yaw angle of helicopter in directional maneuver in hover. The side wind gust of speed V_{gust} = 9 m/s in direction coincident with induced speed of tail rotor. Initially the blade pitch was increased, yaw angle (-) for fuselage nose turn to the left

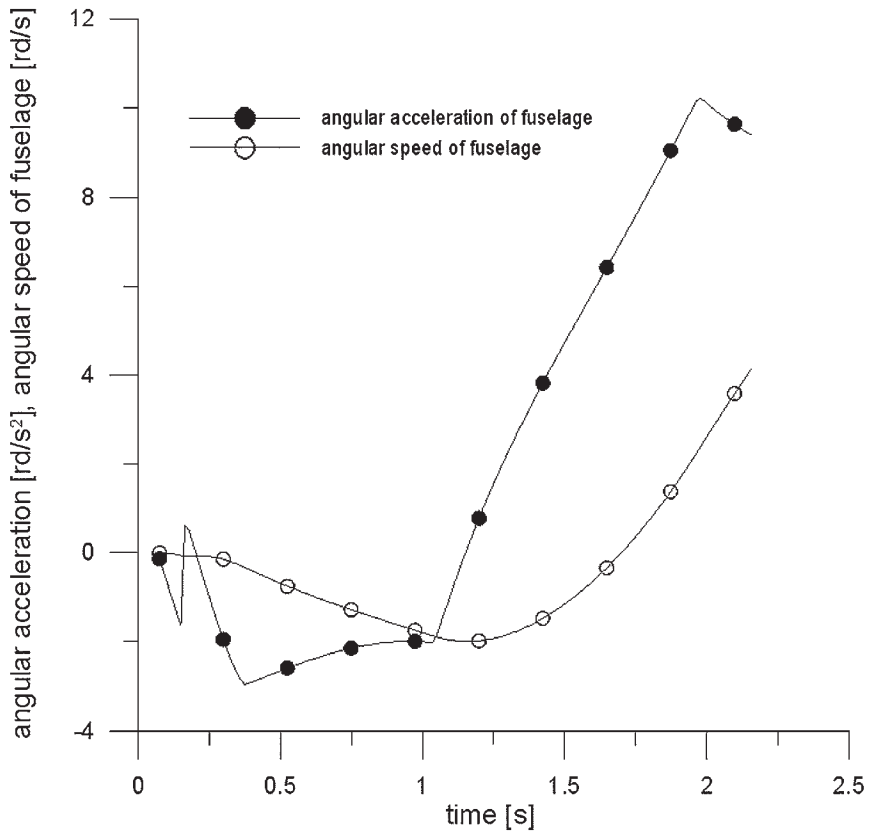

Fig. 24. Angular speed and acceleration of helicopter yawing with rough control of tail rotor blade pitch in directional maneuver in hover. At time t = 0.15 s the side wind gust of speed V_{gust} = 9 m/s was applied in direction coincident with induced speed of tail rotor Initially the blade pitch was increased, angular speed and acceleration (-) for fuselage nose turn to the left

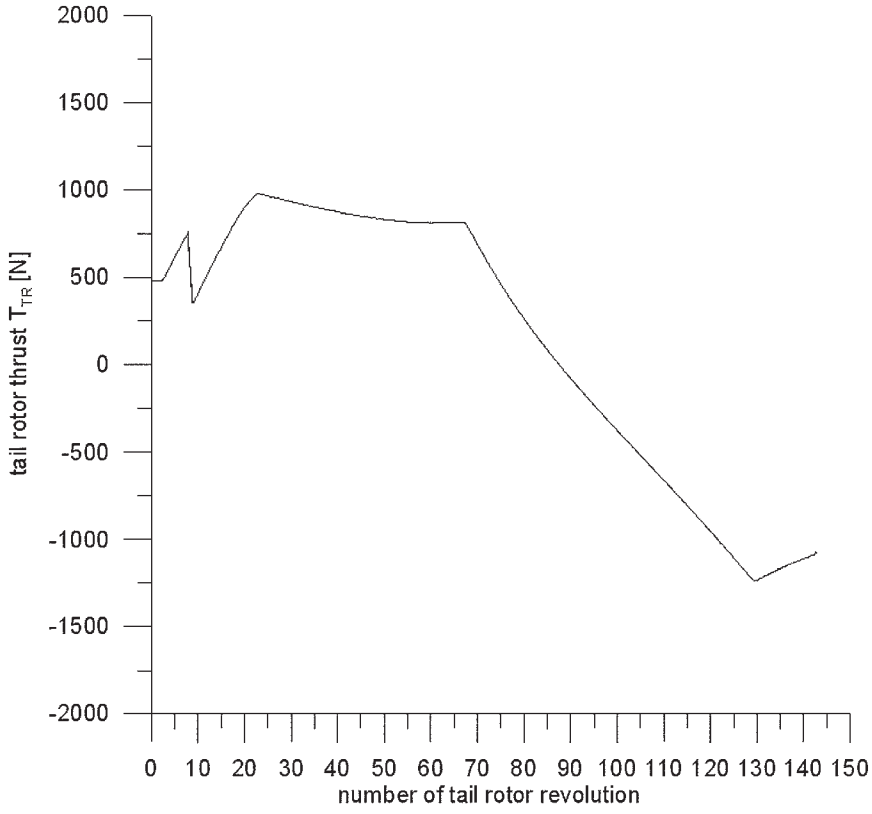

Fig. 25. Tail rotor thrust in directional maneuver in hover with rough control of tail rotor blade pitch and applied the side wind gust of speed V_{gust} = 9 m/s in direction coincident with induced speed of tail rotor. Initially the blade pitch was increased, (+) for tail rotor thrust toward azimuth 90° of the main rotor disk

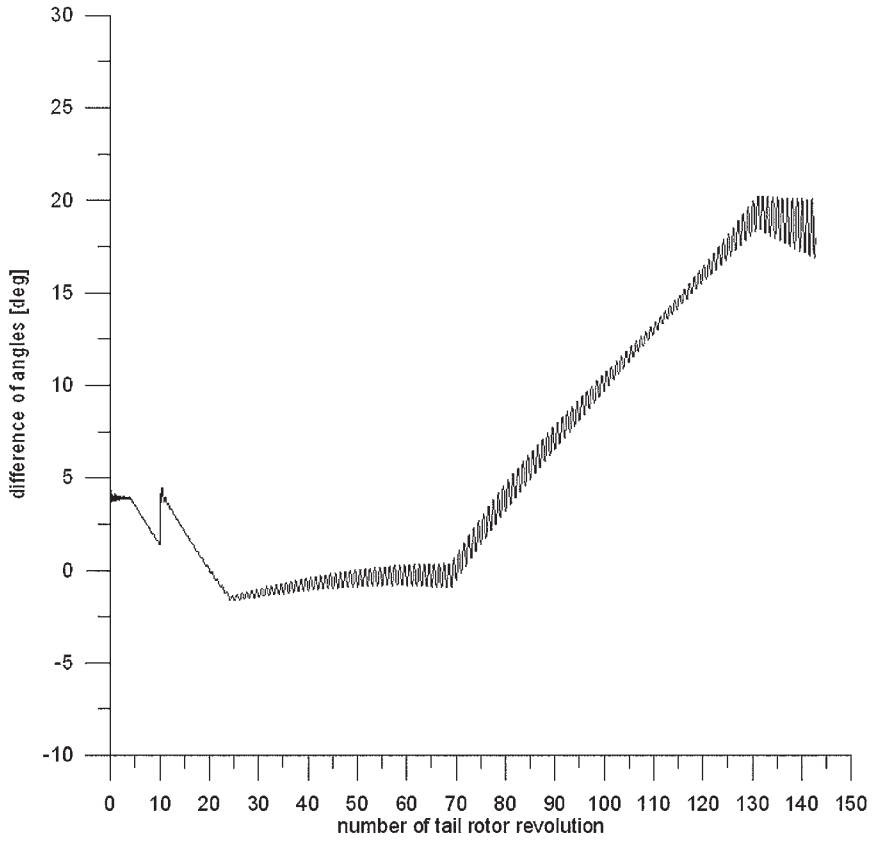

Fig. 26. Differences between stall and local attack angles at blade tip of tail rotor during directional maneuver in hover with rough blade pitch control and applied at 10 th revolution the side wind gust of speed V_{gust} = 9 m/s in direction coincident with induced speed of tail rotor. Initially the blade pitch was increased

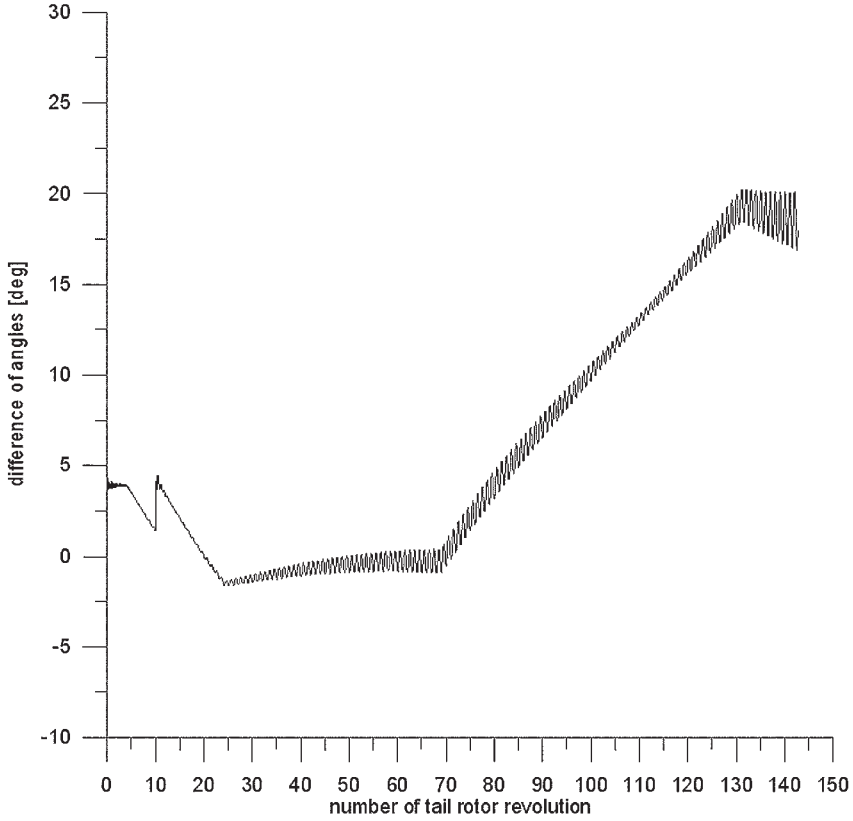

Fig. 27. Torsion angle of blade tip of tail rotor during directional maneuver in hover. Rough blade pitch control and the side wind gust of speed V_{gust} = 9 m/s in direction coincident with induced speed of tail rotor. Initially the blade pitch was increased

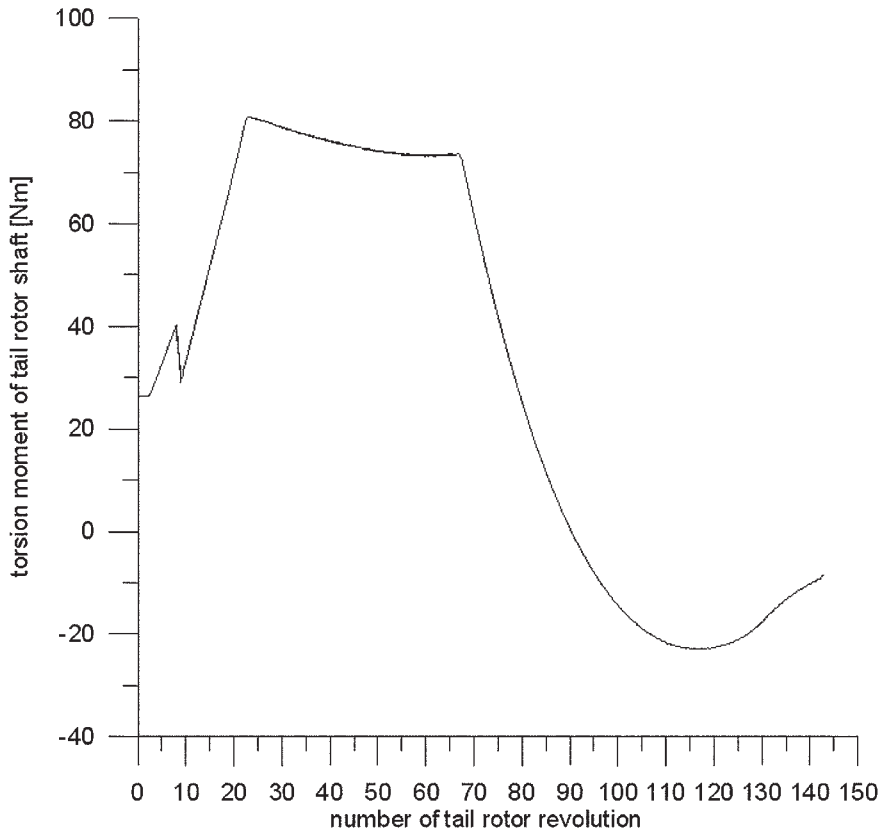

Fig. 28. Torsion moment of tail rotor shaft during directional maneuver in hover with rough blade pitch control and the side wind gust of speed V_{gust} = 9 m/s in direction coincident with induced speed of tail rotor. Initially the blade pitch was increased. Negative value of torsion moment shows the tail rotor autorotation

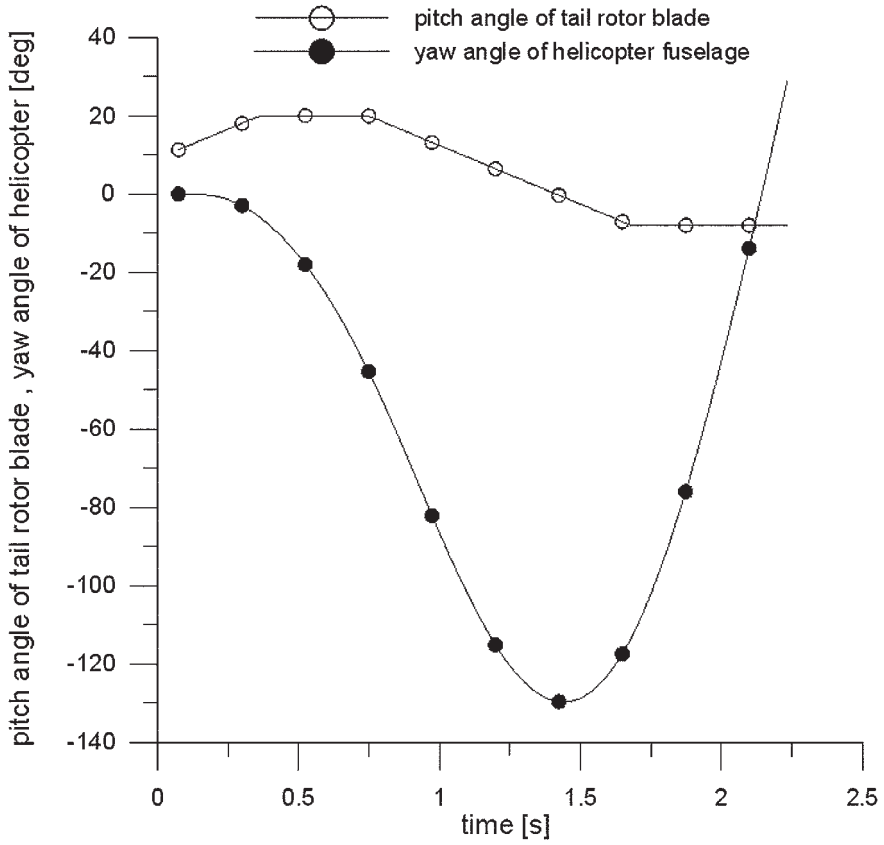

Fig. 29. Function of rough control of pitch angle of tail rotor blade and yaw angle of helicopter in directional maneuver in hover. The side wind gust of speed V_{gust} = -9 m/s in direction opposite to induced speed of tail rotor. Initially the blade pitch was increased, yaw angle (-) for fuselage nose turn to the left

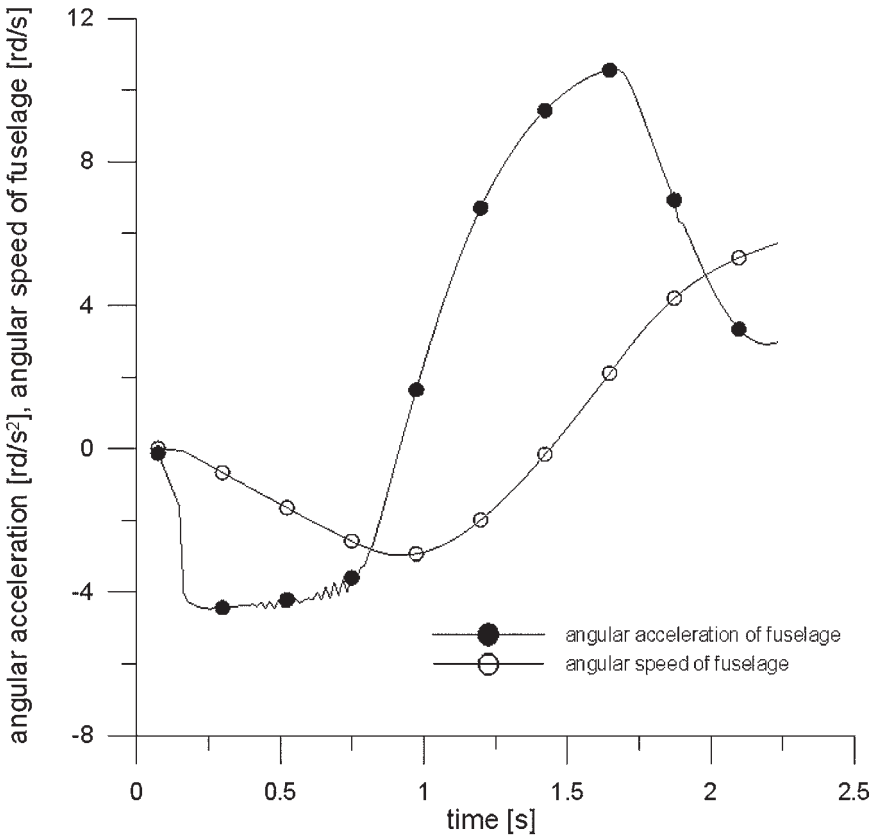

Fig. 30. Angular speed and acceleration of helicopter yawing with rough control of tail rotor blade pitch in directional maneuver in hover. At time t = 0.15 s the side wind gust of speed V_{gust} = -9 m/s was applied in direction opposite to induced speed of tail rotor Initially the blade pitch was increased, angular speed and acceleration (-) for fuselage nose turn to the left

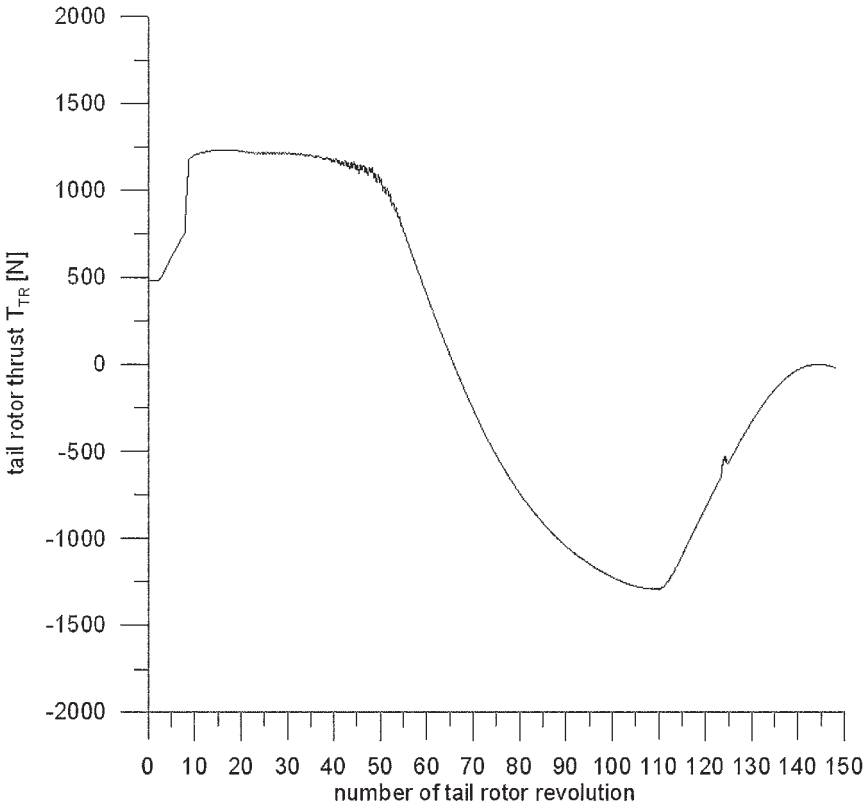

Fig. 31. Tail rotor thrust in directional maneuver in hover with rough control of tail rotor blade pitch and applied the side wind gust of speed V_{gust} = -9 m/s in direction opposite to induced speed of tail rotor. Initially the blade pitch was increased, (+) for tail rotor thrust toward azimuth 90^{o} of the main rotor disk

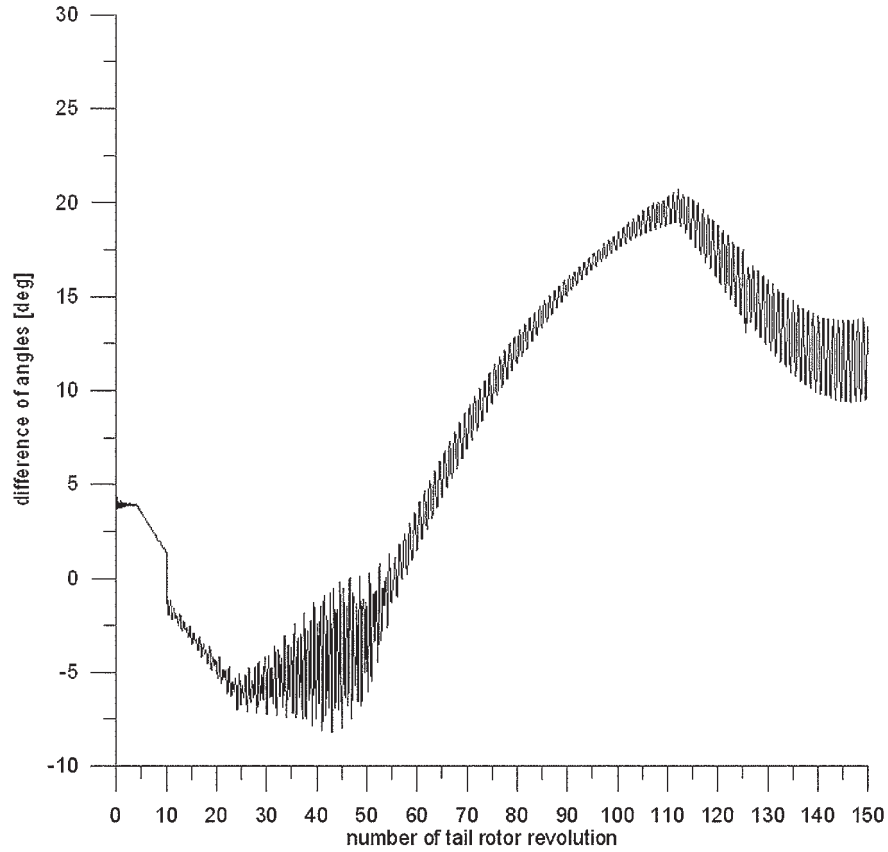

Fig. 32. Differences between stall and local attack angles at blade tip of tail rotor during directional maneuver in hover with rough blade pitch control and applied at 10th revolution the side wind gust of speed V_{gust} = -9 m/s in direction opposite to induced speed of tail rotor. Initially the blade pitch was increased

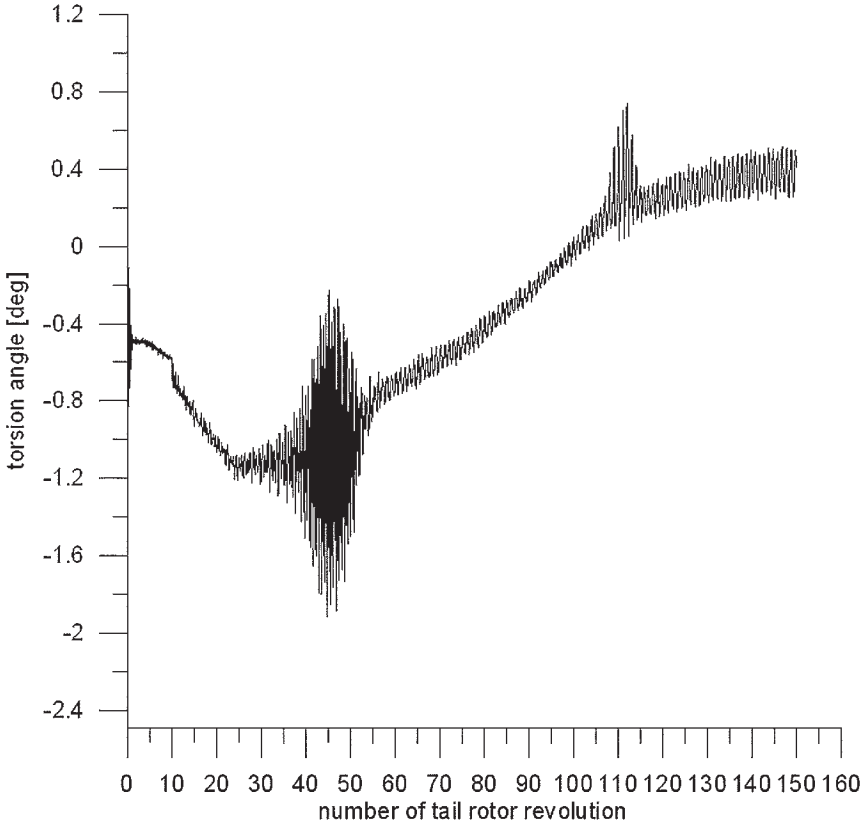

Fig. 33. Torsion angle of blade tip of tail rotor during directional maneuver in hover. Rough blade pitch control and the side wind gust of speed V_{gust} = -9 m/s in direction opposite to induced speed of tail rotor. Initially the blade pitch was increased

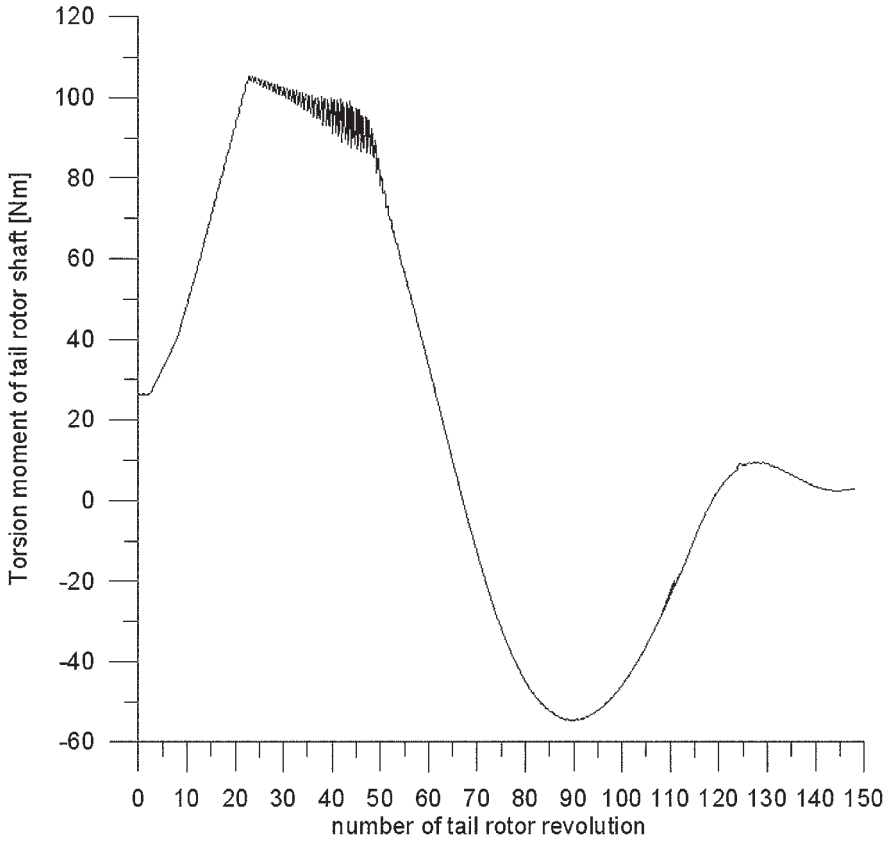

Fig. 34. Torsion moment of tail rotor shaft during directional maneuver in hover with rough blade pitch control and the side wind gust of speed V_{gust} = -9 m/s in direction opposite to induced speed of tail rotor. Initially the blade pitch was increased. Negative value of torsion moment shows the tail rotor autorotation

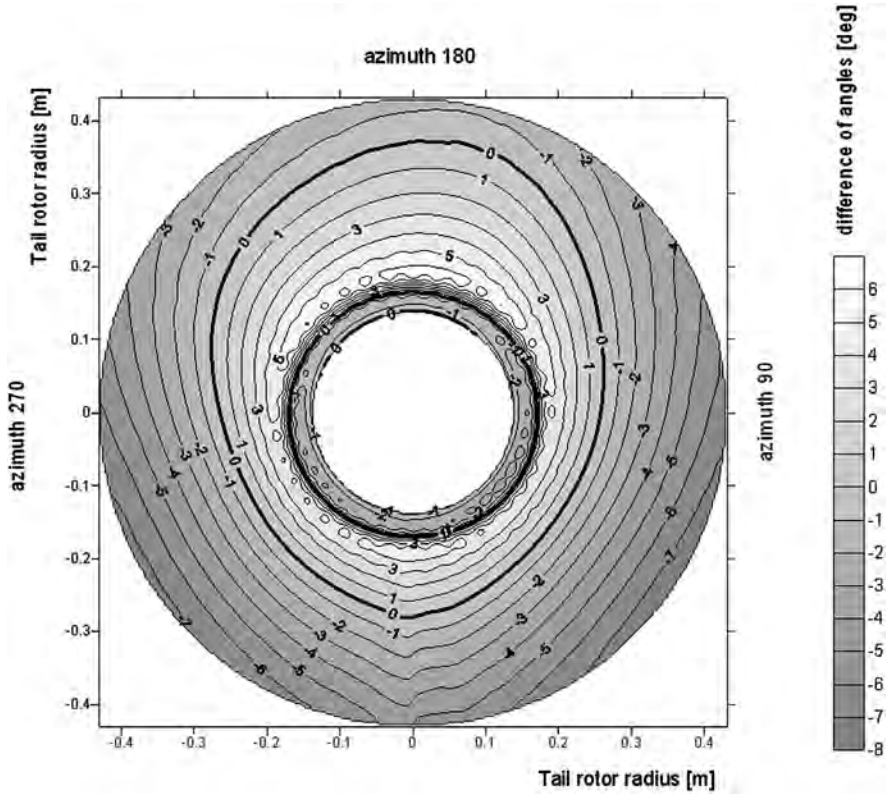

Fig. 35. The differences of stall and local attack angle at the tail rotor disk in directional maneuver with rough blade pitch control and the side wind gust of speed V_{gust} = -9 m/s in direction opposite to induced speed of tail rotor. Map for 40th rotor revolution, the blade tip in deep stall condition at all perimeter of the tail rotor disk. The stall region occurs with the elliptic shape border

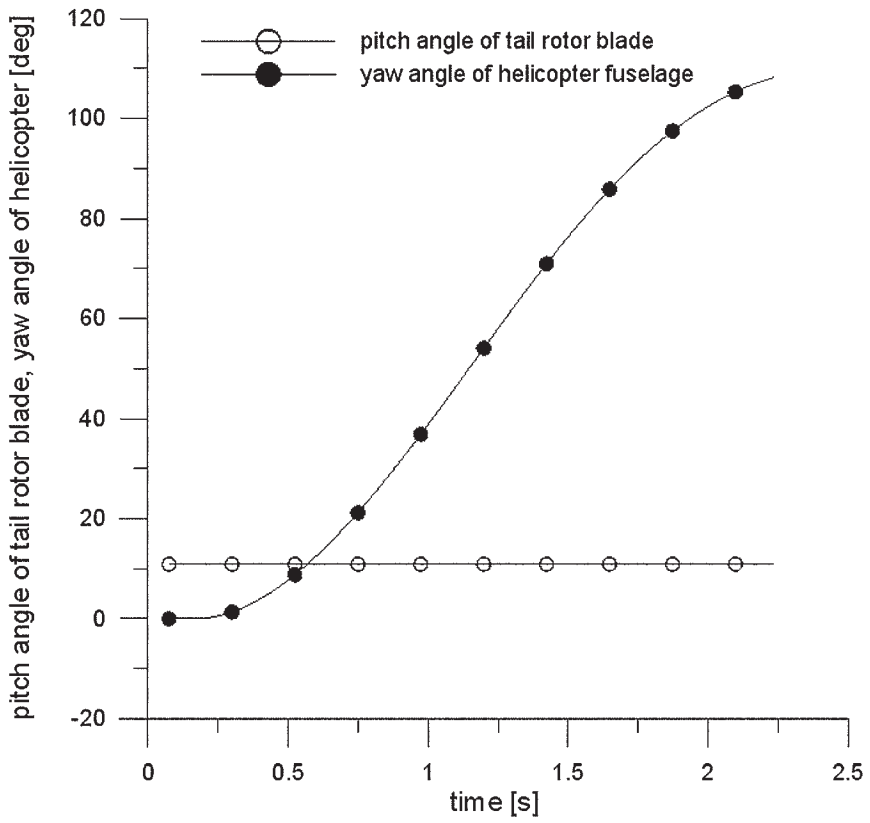

Fig. 36. Function of yaw angle of helicopter in hover for the side wind gust of speed V_{gust} = 9 m/s in direction coincident with induced speed of tail rotor and without pilot reaction. The blade pitch is kept constant, yaw angle (+) for fuselage nose turn to the right

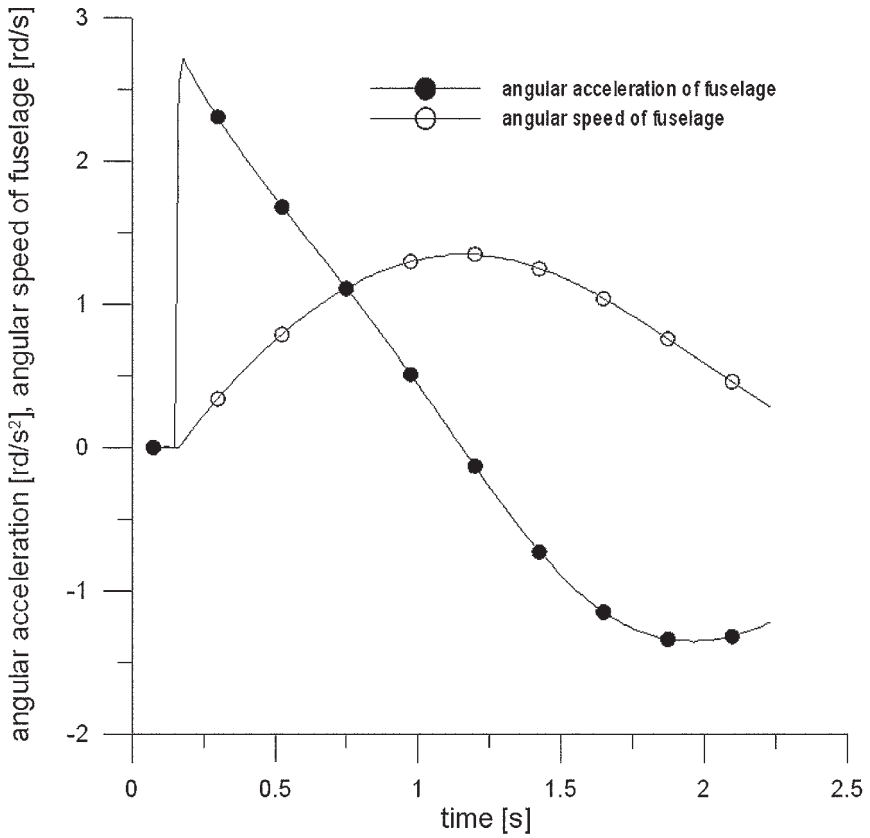

Fig. 37. Angular speed and acceleration of helicopter yawing in hover with at time t = 0.15 s the side wind gust of speed V_{gust} = 9 m/s applied in direction coincident with induced speed of tail rotor and without pilot reaction. The blade pitch is kept constant, angular speed and acceleration (+) for fuselage nose turn to the right

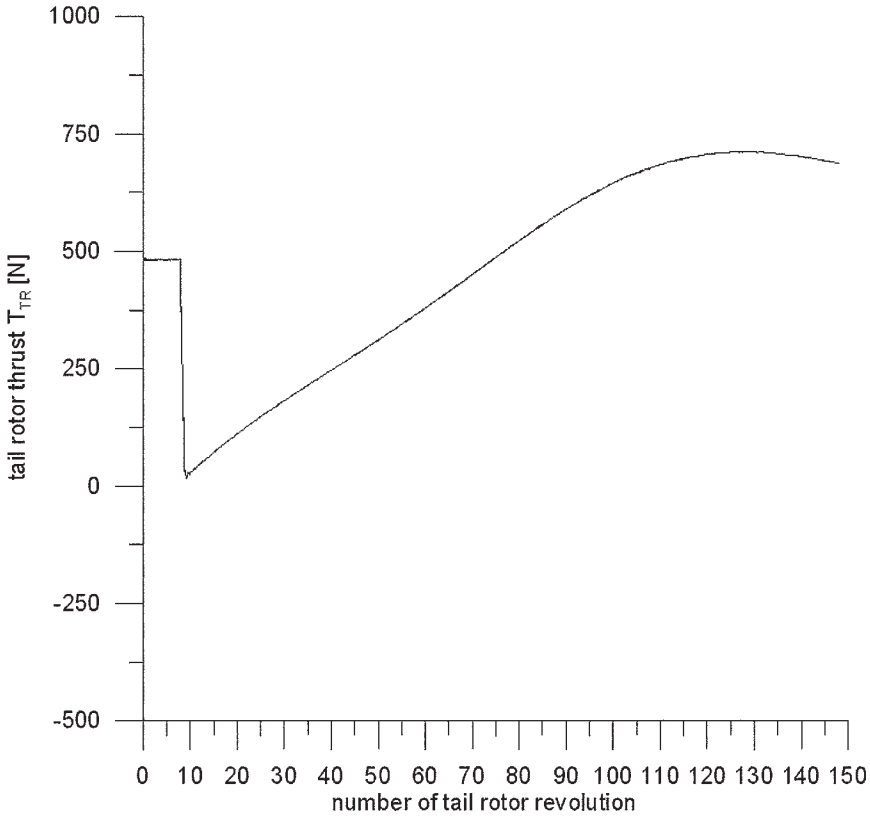

Fig. 38. Tail rotor thrust in hover with the side wind gust of speed V_{gust} = 9 m/s in direction coincident with induced speed of tail rotor and without pilot reaction. The blade pitch is kept constant, (+) for tail rotor thrust toward azimuth 90° of the main rotor disk

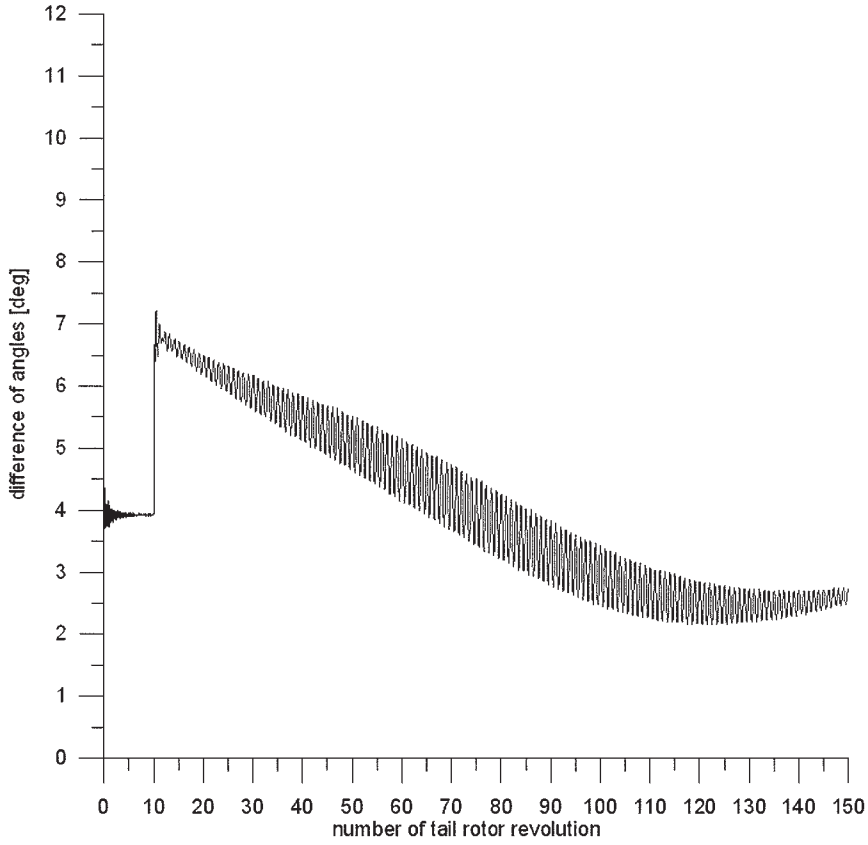

Fig. 39. Differences between stall and local attack angles at blade tip of tail rotor in hover with applied at 10 th revolution the side wind gust of speed V_{gust} = 9 m/s in direction coincident with induced speed of tail rotor. The blade pitch is kept constant

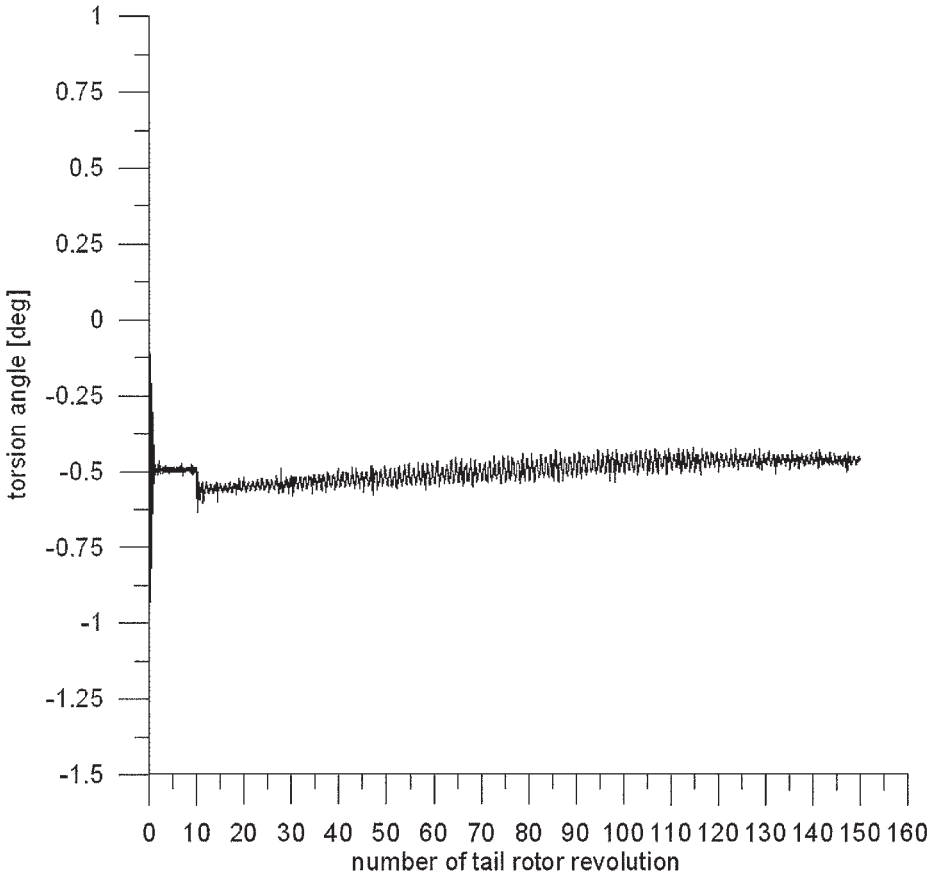

Fig. 40. Torsion angle of blade tip of tail rotor in hover with the side wind gust of speed V_{gust} = 9 m/s in direction coincident with induced speed of tail rotor. The blade pitch is kept constant

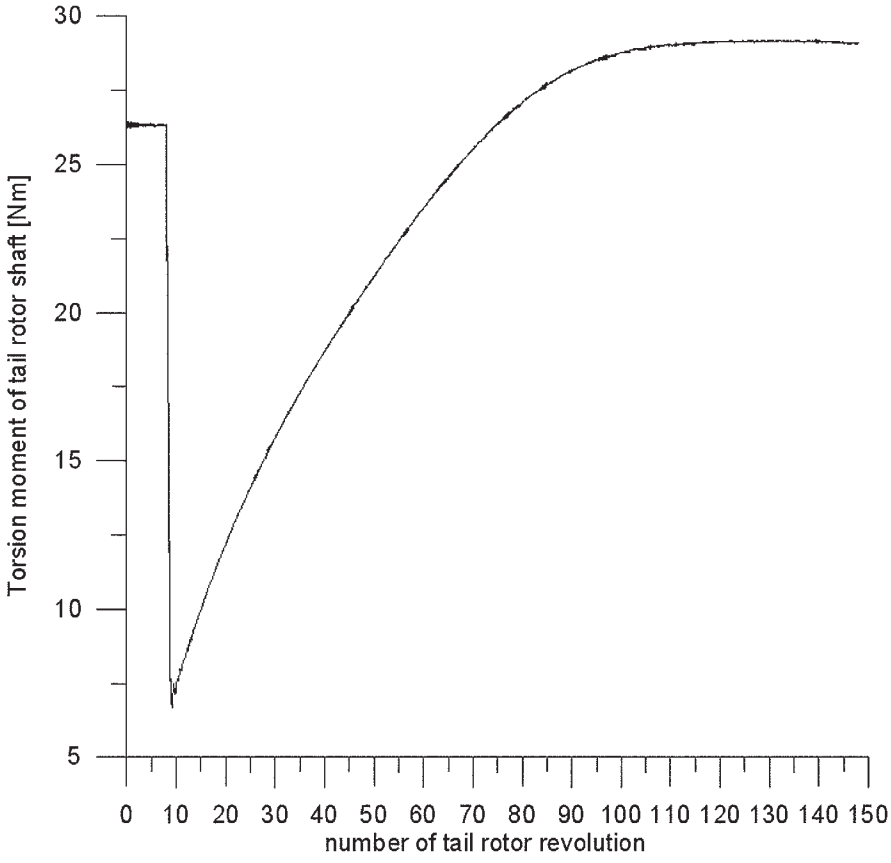

Fig. 41. Torsion moment of tail rotor shaft in hover with the side wind gust of speed V_{gust} = 9 m/s in direction coincident with induced speed of tail rotor. The blade pitch is kept constant

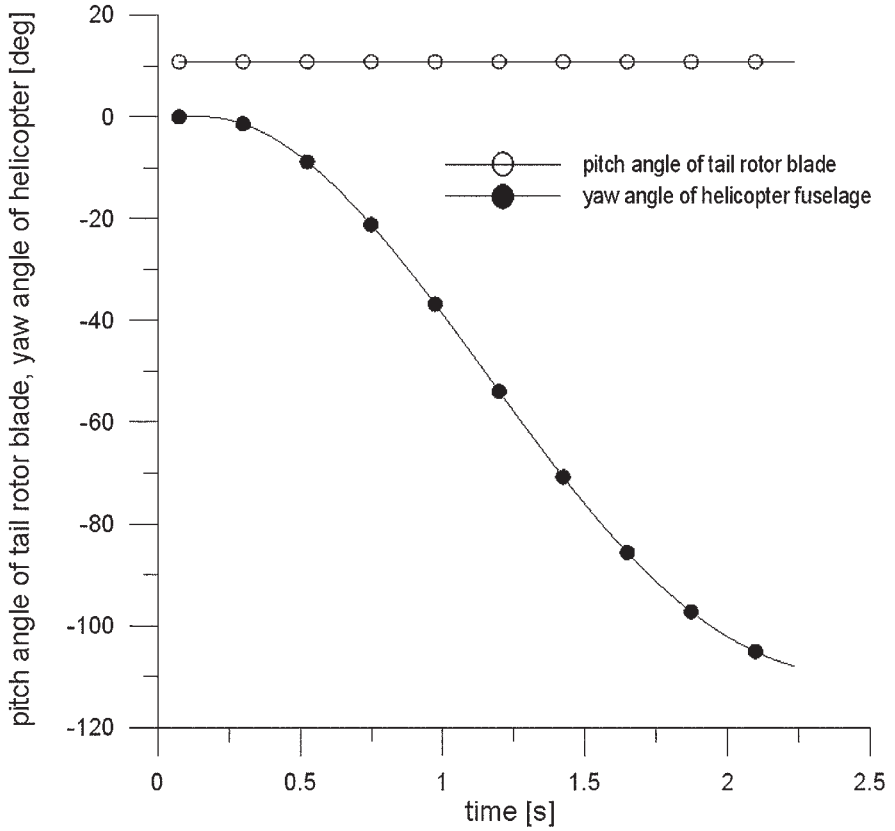

Fig. 42. Function of yaw angle of helicopter in hover for the side wind gust of speed V_{gust} = -9 m/s in direction opposite to induced speed of tail rotor and without pilot reaction. The blade pitch is kept constant, yaw angle (-) for fuselage nose turn to the left

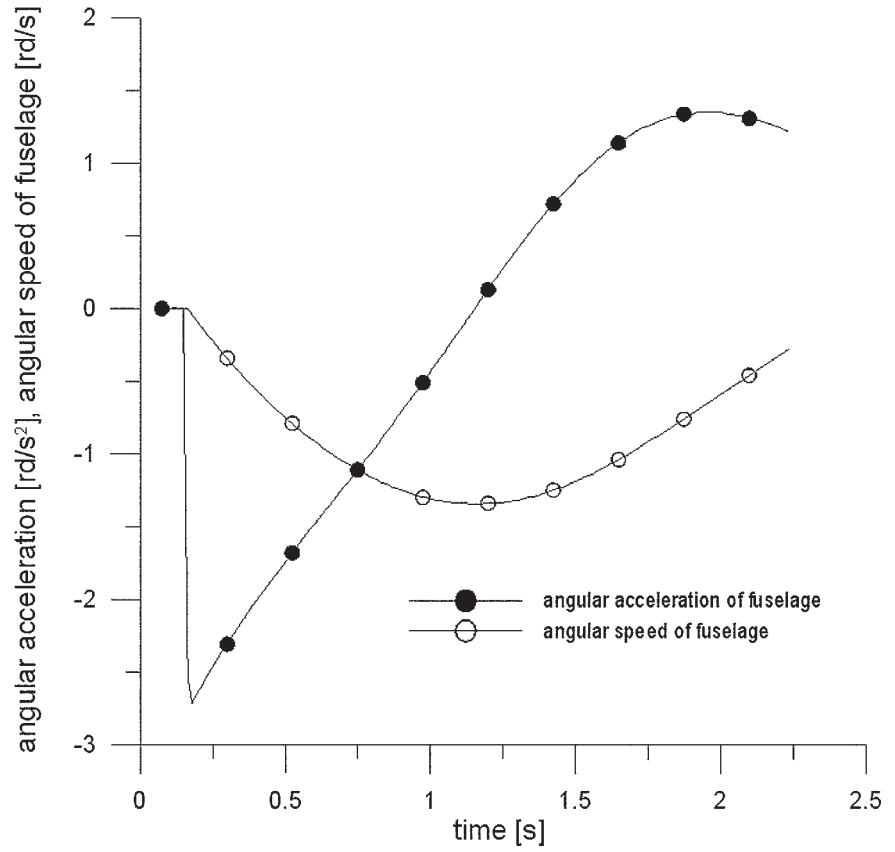

Fig. 43. Angular speed and acceleration of helicopter yawing in hover with at time t = 0.15 s the side wind gust of speed V_{gust} = -9 m/s applied in direction opposite to induced speed of tail rotor and without pilot reaction. The blade pitch is kept constant, angular speed and acceleration (-) for fuselage nose turn to the left

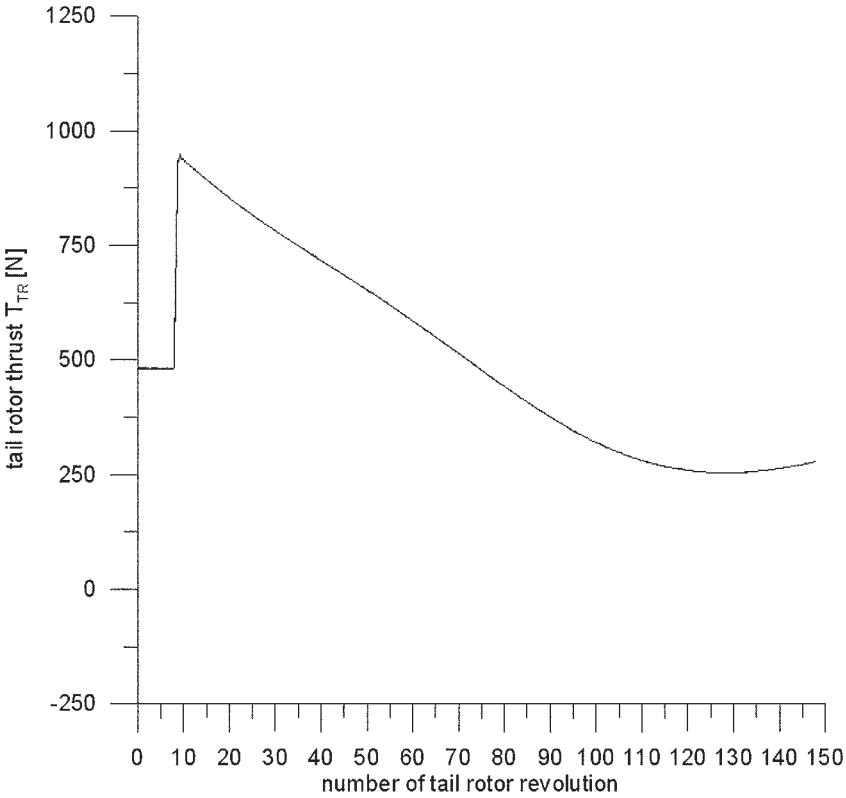

Fig. 44. Tail rotor thrust in hover with the side wind gust of speed V_{gust} = -9 m/s in direction opposite to induced speed of tail rotor and without pilot reaction. The blade pitch is kept constant, (+) for tail rotor thrust toward azimuth 90° of the main rotor disk

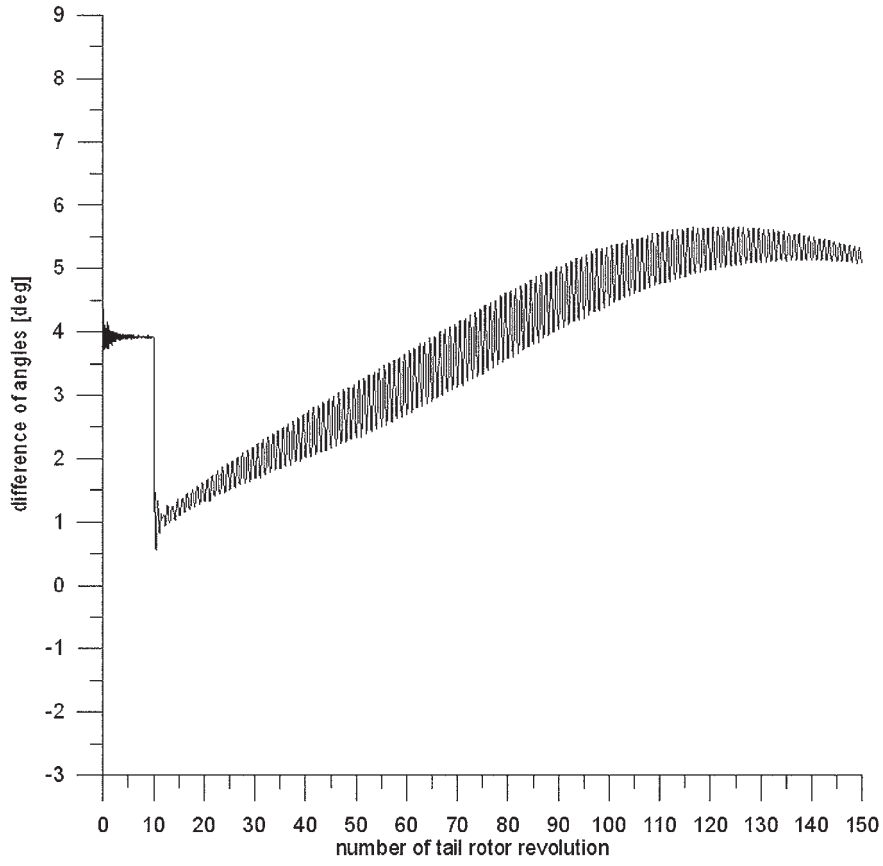

Fig. 45. Differences between stall and local attack angles at blade tip of tail rotor in hover with applied at 10^{th} revolution the side wind gust of speed V_{gust} = -9 m/s in direction opposite to induced speed of tail rotor. The blade pitch is kept constant

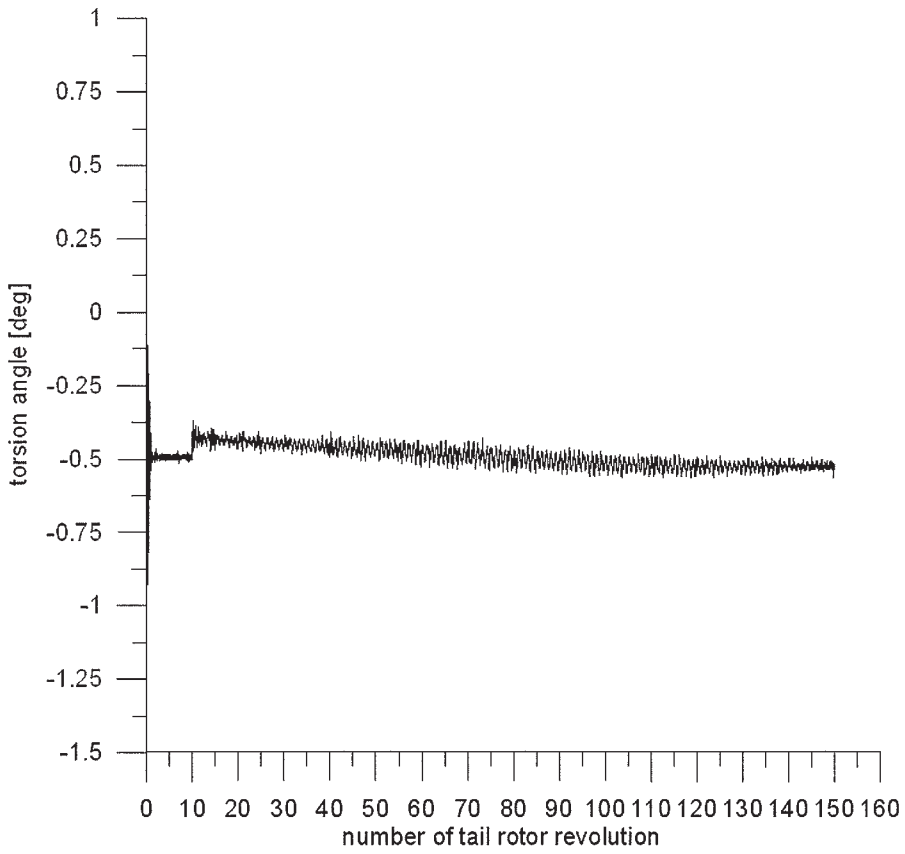

Fig. 46. Torsion angle of blade tip of tail rotor in hover with the side wind gust of speed V_{gust} = -9 m/s in direction opposite to induced speed of tail rotor. The blade pitch is kept constant

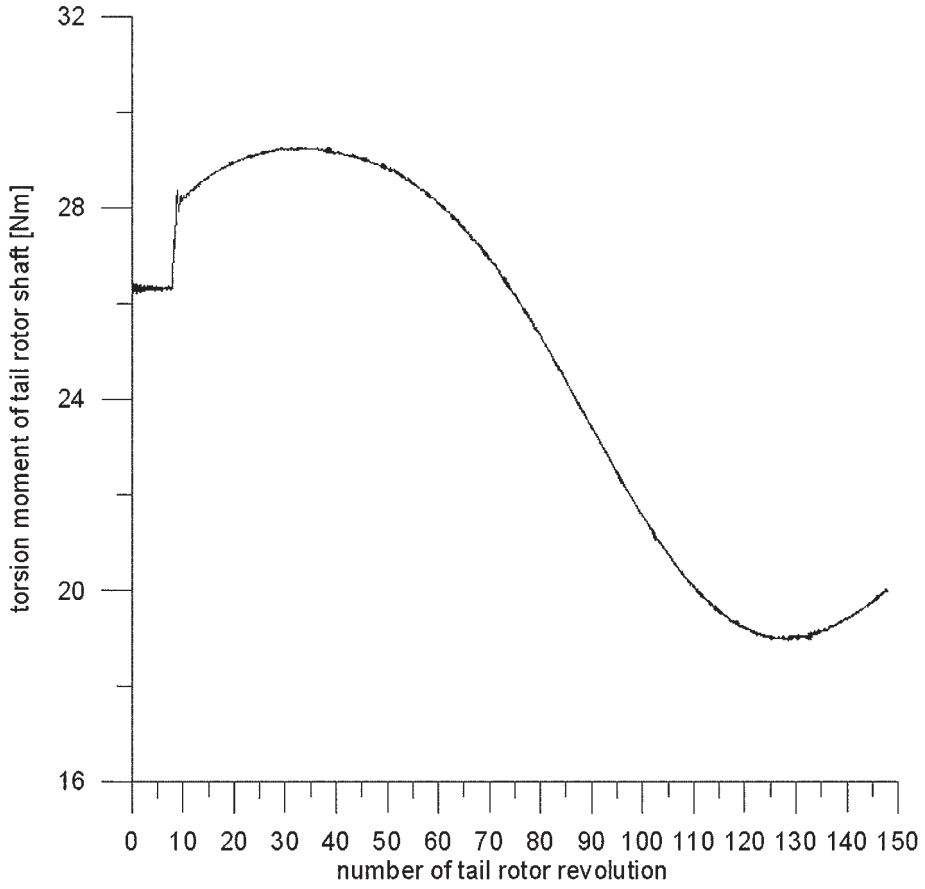

Fig. 47. Torsion moment of tail rotor shaft in hover with the side wind gust of speed V_{gust} = -9 m/s in direction opposite to induced speed of tail rotor. The blade pitch is kept constant

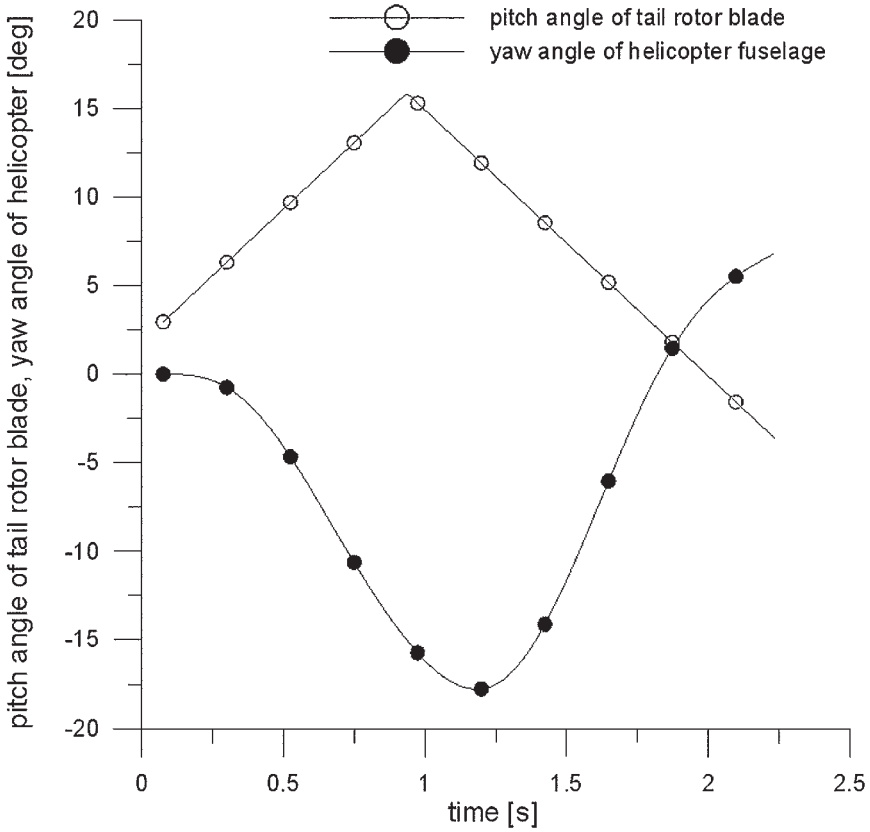

Fig. 48. Function of rough control of pitch angle of tail rotor blade and yaw angle of helicopter in directional maneuver in level flight at speed V = 191 km/h.
Initially the blade pitch was increased, yaw angle (-) for fuselage nose turn to the left

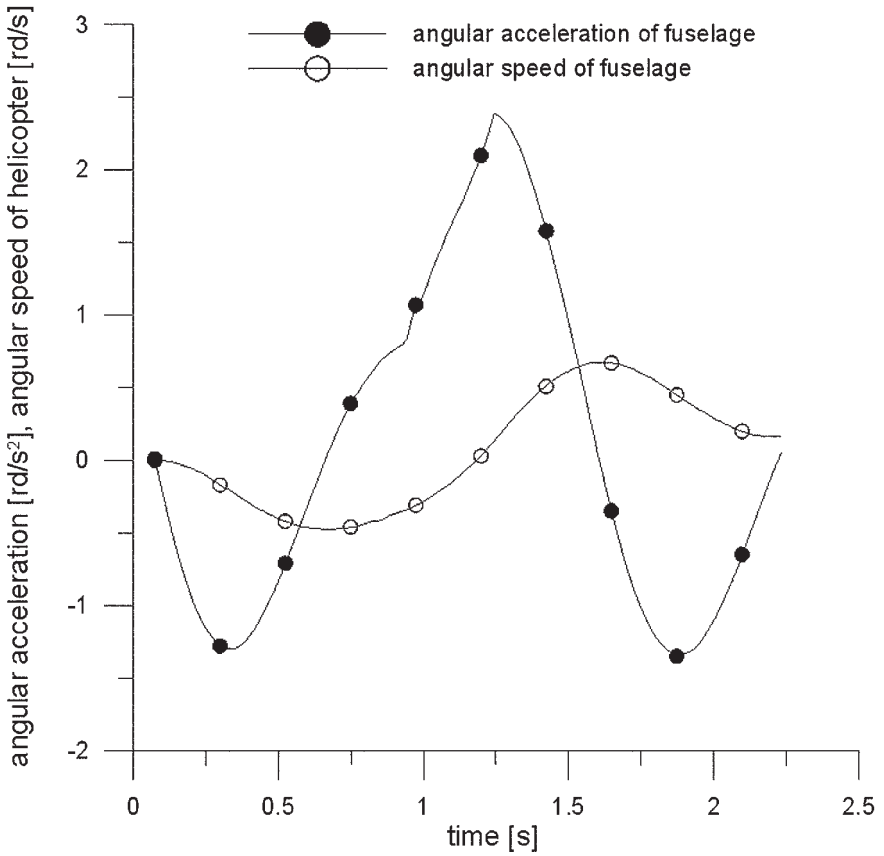

Fig. 49. Angular speed and acceleration of helicopter yawing with rough control of tail rotor blade pitch in directional maneuver in level flight at speed V = 191 km/h.
Initially the blade pitch was increased, angular speed and acceleration (-) for fuselage nose turn to the left

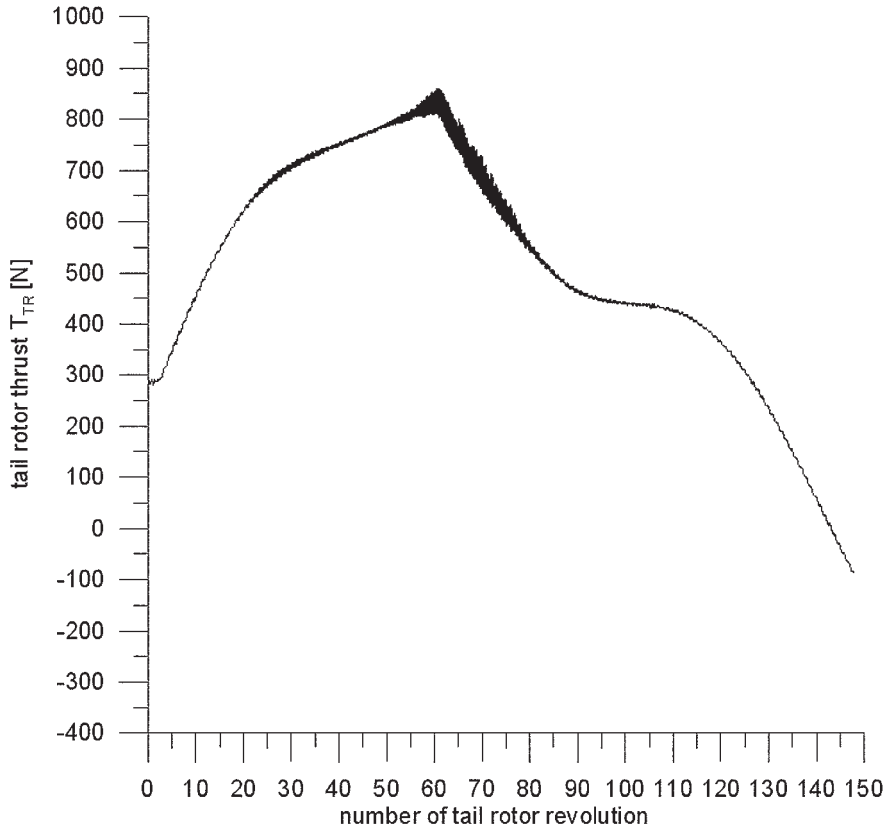

Fig. 50. Tail rotor thrust in directional maneuver with rough control of tail rotor blade pitch in level flight at speed V = 191 km/h. Initially the blade pitch was increased, (+) for tail rotor thrust toward azimuth 90° of the main rotor disk

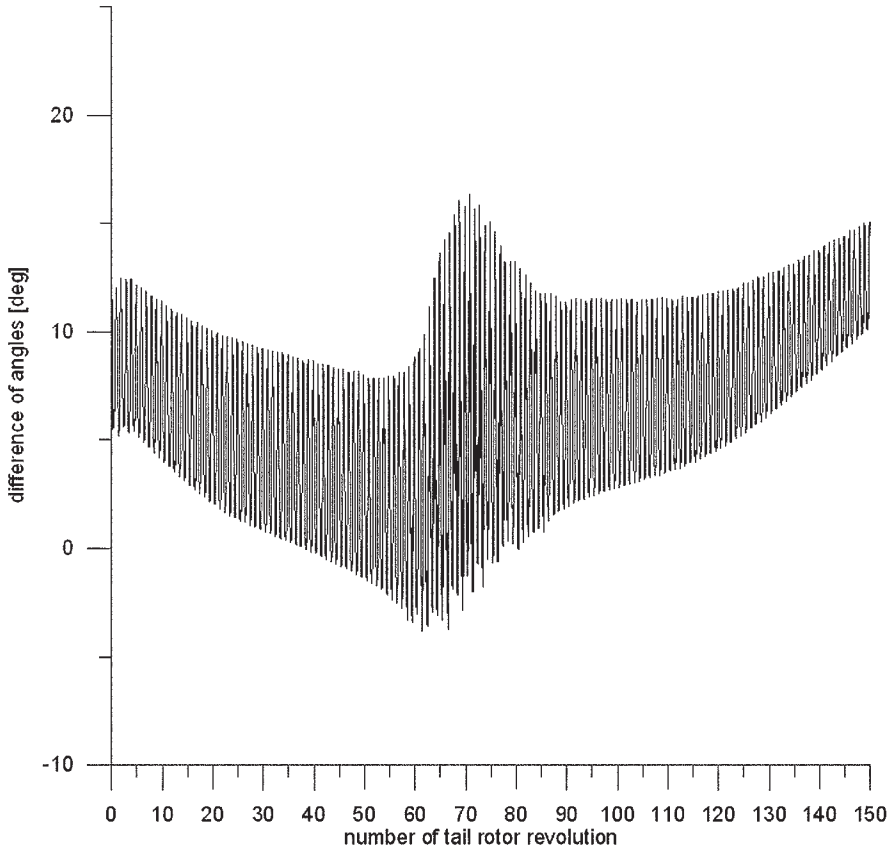

Fig. 51. Differences between stall and local attack angles at blade tip of tail rotor during directional maneuver with rough blade pitch control in level flight at speed V = 191 km/h. Initially the blade pitch was increased. The negative value of difference for stall region

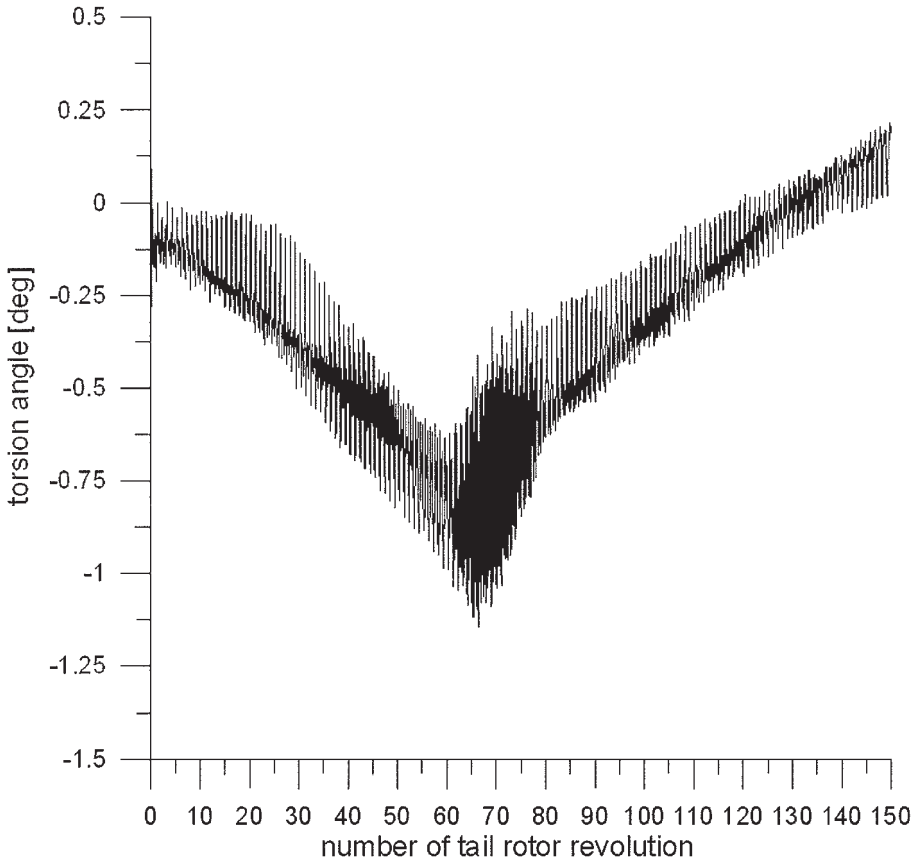

Fig. 52. Torsion angle of blade tip of tail rotor during directional maneuver with rough blade pitch control in level flight at speed V = 191 km/h. Initially the blade pitch was increased

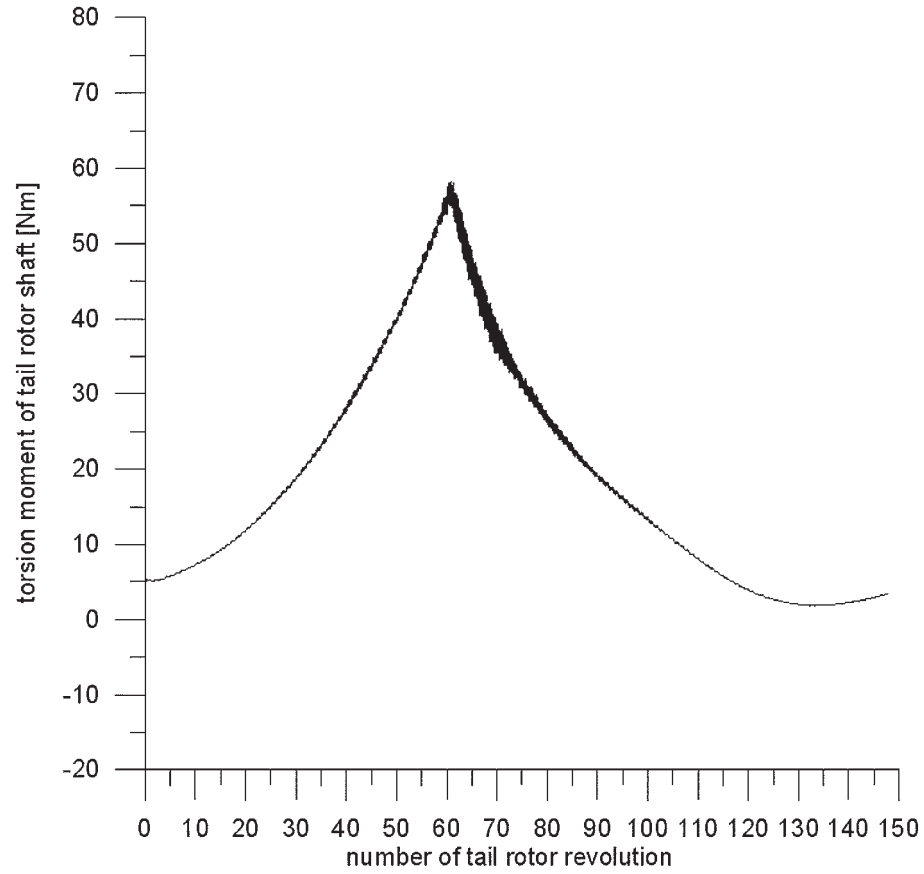

Fig. 53. Torsion moment of tail rotor shaft during directional maneuver with rough blade pitch control in level flight at speed V = 191 km/h. Initially the blade pitch was increased

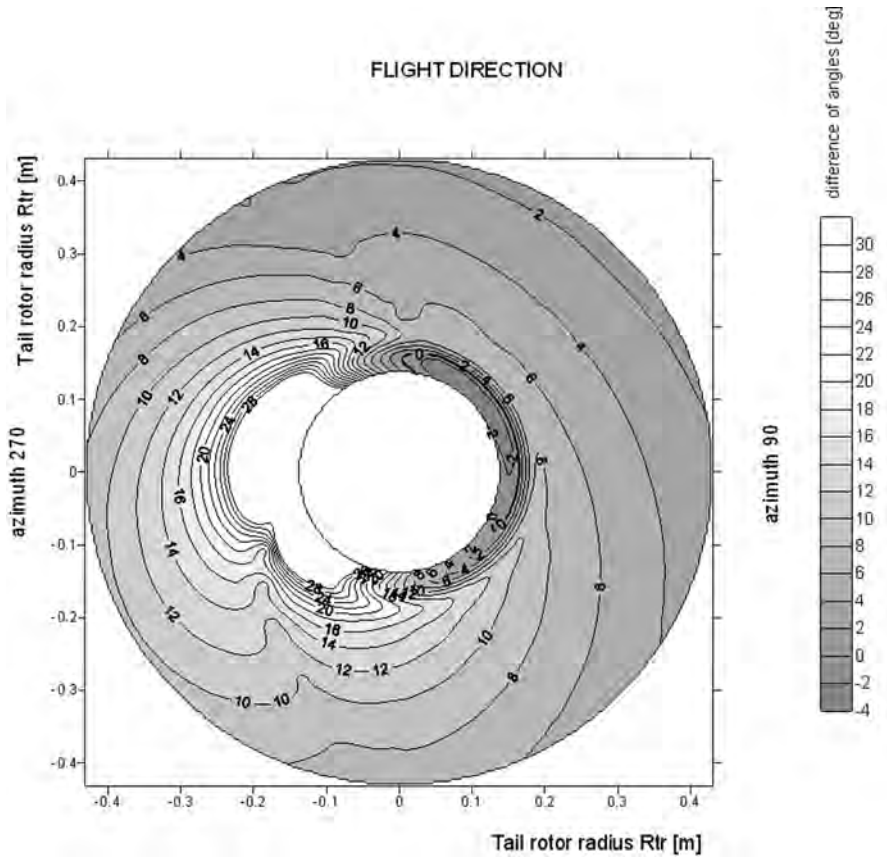

Fig. 54. The differences of stall and local attack angle at the tail rotor disk in directional maneuver with rough blade pitch control in level flight at speed V = 191 km/h. Map for 25th rotor revolution at initial phase of maneuver. There is no stall region at the blade tip of the tail rotor

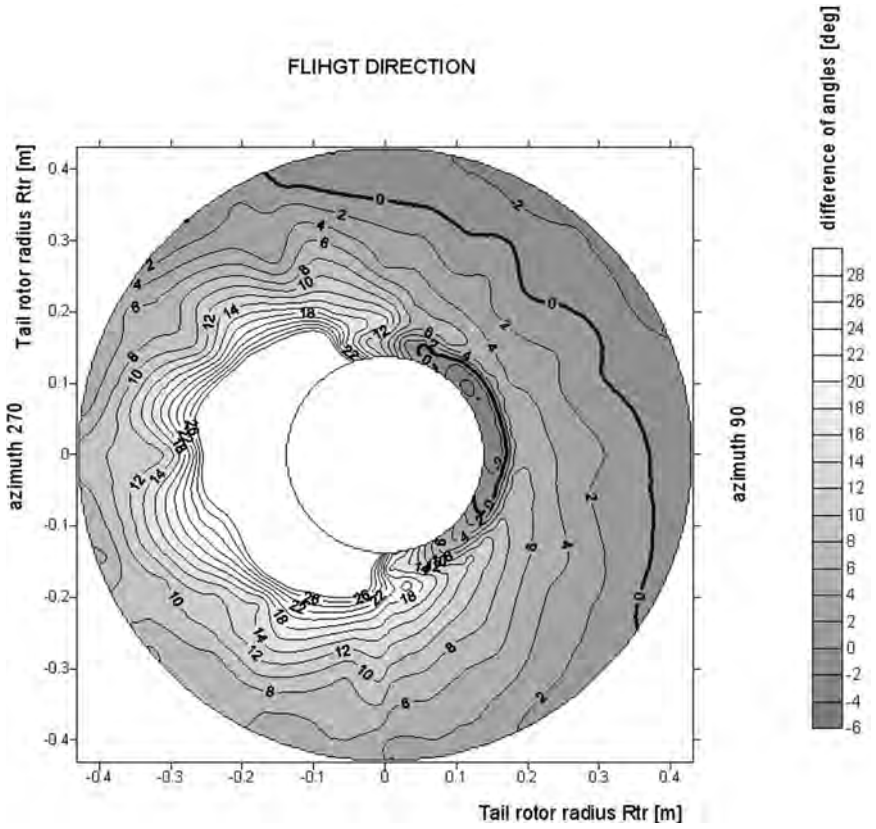

Fig. 55. The differences of stall and local attack angle at the tail rotor disk in directional maneuver with rough blade pitch control in level flight at speed V = 191 km/h. Map for 60th rotor revolution with large stall region from blade position of azimuth 90° to azimuth 180°

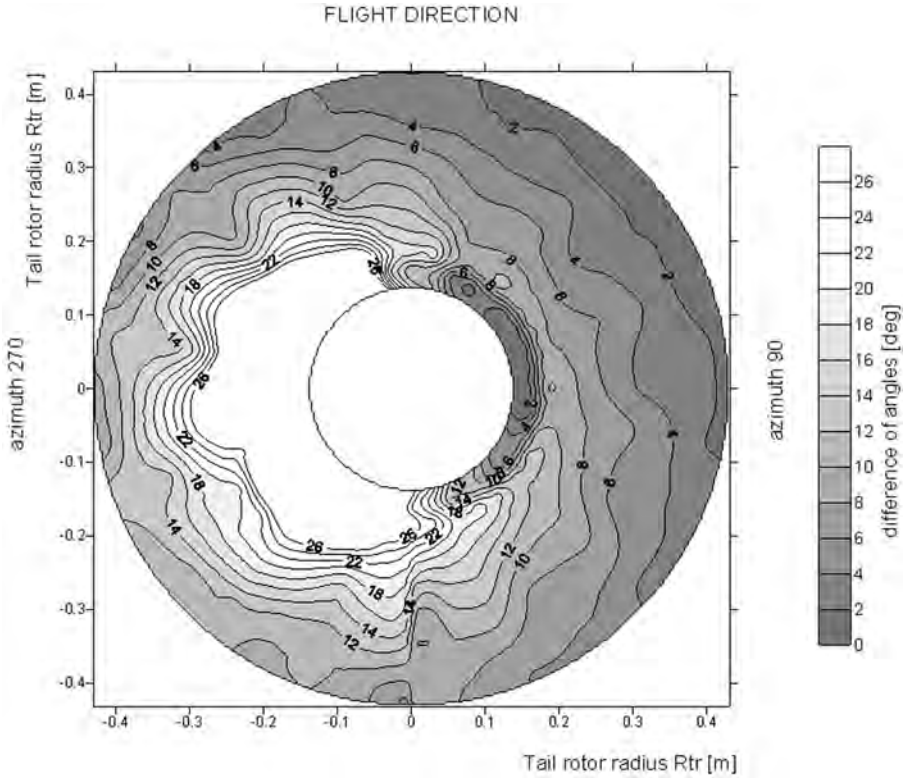

Fig. 56. The differences of stall and local attack angle at the tail rotor disk in directional maneuver with rough blade pitch control in level flight at speed V = 191 km/h. Map for 81st rotor revolution where despite lack of stall region the influence of blade oscillating motion is visible

BIBLIOGRAPHY

[1] **Learmount D.**: *Sting in the tail.* Flight International, 9-15 March 2004, s. 40-41.

[2] **Tarttelin P. C.**: *Tail rotor failure – what can be done? An engineering approach*. 26th European Rotorcraft Forum, Hague, Netherlands, 26-29 September 2000.

[3] **Stanisławski J.**: *Symulacyjne badanie spadku aerodynamicznej efektywności śmigła ogonowego śmigłowca*. Sprawozdanie Instytutu Lotnictwa 06/BP/2005, Warszawa 2005.

[4] **Stanisławski J.**: *Instrukcje użytkowania programów komputerowych dotyczących zagadnień mechaniki lotu śmigłowca i obciążeń łopat wirnika nośnego*. Sprawozdanie Instytutu Lotnictwa GR/01/BP/2004, Warszawa 2004.

[5] **Czechyra T.**: *Badanie wpływu zaburzeń kształtu powierzchni na osiągi statków powietrznych*. Sprawozdanie Instytutu Lotnictwa 85/BA/04, Warszawa 2004.

[6] *Badania tunelowe charakterystyk aerodynamicznych zmodyfikowanego profilu ILHX4A-12M o grubości 12% do śmigłowca IS-2*. Sprawozdanie Instytutu Lotnictwa 117/BA/95, Warszawa 1995.

[7] *Obliczenia charakterystyk aerodynamicznych profilu śmigłowcowego o grubości względnej 9% na wirnik śmigłowca IS-2*. Sprawozdanie Instytutu Lotnictwa 115/BA/95, Warszawa 1995.

[8] *Wstępne badania aerodynamiczne modelu lekkiego śmigłowca IS-2. Badania w tunelu Ø 1,5m*. Sprawozdanie Instytutu Lotnictwa 114/BA/95/D-I, Warszawa 1995.

[9] *Wstępne badania aerodynamiczne modelu lekkiego śmigłowca IS-2. Badania w tunelu Ø 1,5m. Część II-Stateczność kierunkowa*. Sprawozdanie Instytutu Lotnictwa 114/BA/95/D-II, Warszawa 1996.

[10] *Zadanie techniczne na projektowanie łopaty śmigła ogonowego śmigłowca IS-2*. Dok. Nr IS-29-0006/0, Instytut Lotnictwa, Warszawa 1995.

J. Stanisławski

BADANIA SYMULACYJNE ZACHOWANIA WIRNIKA OGONOWEGO W MANEWRZE KIERUNKOWYM ŚMIGŁOWCA

Streszczenie

Przedstawiono symulacyjną metodę obliczania obciążeń wirnika ogonowego oraz odkształceń jego łopat w trakcie wykonywania manewru kierunkowego śmigłowca. Parametry odchylania określano przy wykorzystaniu uproszczonego równania śmigłowca. W modelu fizycznym uwzględniono sztywną bryłę kadłuba oraz odkształcalne łopaty wirnika ogonowego reprezentowane przez osie sprężyste z układem rozłożonych mas skupionych. Wprowadzenie funkcji zmian kąta nastawienia łopat wirnika ogonowego z uwzględnieniem brutalnego sterowania pozwoliło analizować obciążenia łopat w przypadku występowania rozległych stref oderwania.

Я. Станиславски

СИМУЛЯЦИОННЫЕ ИССЛЕДОВАНИЯ ПОВЕДЕНИЯ ХВОСТОВОГО ВИНТА ВО ВРЕМЯ МАНЁВРА ПО НАПРАВЛЕНИИ ПОЛЁТА

Резюме

Представлен симуляционный метод рассчёта нагрузки хвостового винта и деформаций его лопастей во время реализации вертолётом манёвра по направлении полёта. Параметры отклонения были определены с помощью упрощенного уравнения вертолёта. В физической модели учитывались жёсткое тело фюзеляжа и подлежащие дефортации лопасти хвостового винта, которые представлялись как упругие оси с распределёнными, сосредоточенными массами. Введение функции изменений угла атаки лопастей хвостового винта с учётом „грубого" управления, позволило анализировать нагрузки лопастей в случае появления больших районов отрыва.